The Journal of Physiology

Altered adrenergic response in myocytes bordering a chronic myocardial infarction underlies *in vivo* triggered activity and repolarization instability

Eef Dries[1], Matthew Amoni[1], Bert Vandenberk[1], Daniel M. Johnson[1,2], Guillaume Gilbert[1], Chandan K. Nagaraju[1], Rosa Doñate Puertas[1], Mouna Abdesselem[1], Demetrio J. Santiago[1,3], H. Llewelyn Roderick[1], Piet Claus[1], Rik Willems[1] and Karin R. Sipido[1]

[1] *Experimental Cardiology, University of Leuven, Herestraat 49 box 911, Leuven, Belgium*
[2] *Institute of Cardiovascular Sciences, University of Birmingham, Edgbaston, Birmingham B15 2TT, UK*
[3] *Laboratory of Molecular Cardiology, Centro Nacional de Investigaciones Cardiovasculares Carlos III (CNIC), C. Melchor Fernández Almagro 3, 28029, Madrid, Spain*

Edited by: Harold Schultz & Tania Zaglia

Key points

- Ventricular arrhythmias are a major complication after myocardial infarction (MI), associated with sympathetic activation. The structurally heterogeneous peri-infarct zone is a known substrate, but the functional role of the myocytes is less well known.
- Recordings of monophasic action potentials *in vivo* reveal that the peri-infarct zone is a source of delayed afterdepolarizations (DADs) and has a high beat-to-beat variability of repolarization (BVR) during adrenergic stimulation (isoproterenol, ISO).
- Myocytes isolated from the peri-infarct region have more DADs and spontaneous action potentials, with spontaneous Ca^{2+} release, under ISO. These myocytes also have reduced repolarization reserve and increased BVR. Other properties of post-MI remodelling are present in both peri-infarct and remote myocytes.
- These data highlight the importance of altered myocyte adrenergic responses in the peri-infarct region as source and substrate of post-MI arrhythmias.

Abstract Ventricular arrhythmias are a major early complication after myocardial infarction (MI). The heterogeneous peri-infarct zone forms a substrate for re-entry while arrhythmia initiation is often associated with sympathetic activation. We studied the mechanisms triggering these post-MI arrhythmias *in vivo* and their relation to regional myocyte remodelling. In pigs with chronic MI (6 weeks), *in vivo* monophasic action potentials were simultaneously recorded in the

Eef Dries is a postdoctoral researcher at the University of Leuven (Belgium). Her research focuses on defective Ca^{2+} handling and underlying mechanisms in arrhythmias in large animal models and human heart failure patients. Her current research interest is to investigate the impact of cellular interactions on arrhythmia mechanisms in multicellular tissue preparations. **Matthew Amoni** is an MD-PhD student at the University of Leuven (Belgium). He obtained his medical degree, and concurrently a masters' degree, from the University of Cape Town (South Africa). His research is focused on the mechanisms of post-infarction arrhythmogenesis, with special interest in the vulnerable infarct border zone. His ongoing work explores an integration of *in vivo* mapping and cellular electrophysiology techniques.

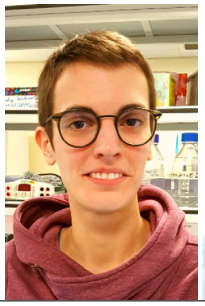

E. Dries and M. Amoni contributed equally to this work.

DOI: 10.1113/JP278839

peri-infarct and remote regions during adrenergic stimulation with isoproterenol (isoprenaline; ISO). Sham animals served as controls. During infusion of ISO *in vivo*, the incidence of delayed afterdepolarizations (DADs) and beat-to-beat variability of repolarization (BVR) was higher in the peri-infarct than in the remote region. Myocytes isolated from the peri-infarct region, in comparison to myocytes from the remote region, had more DADs, associated with spontaneous Ca^{2+} release, and a higher incidence of spontaneous action potentials (APs) when exposed to ISO (9.99 ± 4.2 *vs.* 0.16 ± 0.05 APs/min, $p = 0.004$); these were suppressed by CaMKII inhibition. Peri-infarct myocytes also had reduced repolarization reserve and increased BVR (26 ± 10 ms *vs.* 9 ± 7 ms, $P < 0.001$), correlating with DAD activity. In contrast to these regional distinctions under ISO, alterations in Ca^{2+} handling at baseline and myocyte hypertrophy were present throughout the left ventricle (LV). Expression of some of the related genes was, however, different between the regions. In conclusion, altered myocyte adrenergic responses in the peri-infarct but not the remote region provide a source of triggered activity *in vivo* and of repolarization instability amplifying the substrate for re-entry. These findings stimulate further exploration of region-specific therapies targeting myocytes and autonomic modulation.

(Received 29 August 2019; accepted after revision 1 January 2020; first published online 3 January 2020)
Corresponding author K. R. Sipido: Division of Experimental Cardiology, Department of Cardiovascular Sciences KU Leuven, Campus Gasthuisberg, Herestraat 49 box 911, B-3000 Leuven, Belgium. Email: karin.sipido@kuleuven.be

Introduction

Sudden cardiac death, attributable to ventricular arrhythmia (ventricular fibrillation and tachycardia), is a leading cause of death worldwide, and a common complication after myocardial infarction (MI) (Hayashi *et al.* 2015). The infarct and adjacent border zone, consisting of strands of surviving myocytes interspersed with fibrous tissue, create a structural substrate for re-entry circuits, that are central to post-MI arrhythmias (De Bakker *et al.* 1993; Ashikaga *et al.* 2007).

In addition to the structural substrate of the peri-infarct region, inhomogeneity of repolarization in the surviving myocardium could facilitate re-entry (Ciaccio *et al.* 2018). Experimental studies in small animal models have identified action potential (AP) changes and reduced repolarization reserve in myocytes isolated from the non-infarcted tissue of the left ventricle (LV) (Wong *et al.* 1982; Aimond *et al.* 1999). In mouse models, information regarding differential remodelling in different regions is scarce, though a recent study identified specific transcriptional profiles (van Duijvenboden *et al.* 2019). Data from large animal models support a role for abnormal myocyte repolarization in the peri-infarct region contributing to the functional re-entry substrate (Lue & Boyden, 1992; Baba *et al.* 2005; Sasano *et al.* 2006; Hegyi *et al.* 2018). However, direct evidence, in particular *in vivo*, for a distinct arrhythmogenic repolarization profile in this region, different from the overall post-MI remodelling in the first weeks after MI, is limited.

In clinical practice, the vulnerable substrate is identified through programmed stimulation using premature stimuli as the simulated arrhythmia triggers. With this approach, the MI border zone is often found to be the culprit site and is a common target for ablation post-MI to prevent lethal arrhythmias (Verma *et al.* 2005; Ashikaga *et al.* 2007; Cronin *et al.* 2019). More recently, computational modelling using structural information and simulated triggers could reproduce *in vivo* studies and identify the vulnerable substrate for ablation (Prakosa *et al.* 2018).

Compared to the body of knowledge on the substrate for re-entry, much less is known about the cellular mechanisms triggering *in vivo* post-MI arrhythmias. Premature ventricular complexes (PVC) are most commonly the initiating event, as observed in recordings from intracardiac devices and monitoring studies (Saeed *et al.* 2000; Lerma *et al.* 2013). *In vivo* studies have localized PVCs to the border zone (Marrouche *et al.* 2004), and or correlated their site of origin to the critical exit site of the re-entry circuit, marking these sites for ablation (Bogun *et al.* 2008). A number of studies using isolated tissues have implicated spontaneous depolarizations and automaticity from Purkinje fibres with abnormal potentials (Xing & Martins, 2004; Bogun *et al.* 2006; Hirose *et al.* 2008). Using isolated myocytes, other studies have implicated triggered activity due to delayed afterdepolarizations (DADs) and Ca^{2+} handling abnormalities in the border zone (Baba *et al.* 2005; Belevych *et al.* 2012; Hegyi *et al.* 2018). However, the contribution of such DADs to triggered activity *in vivo* is poorly documented as it requires sophisticated experimentation using monophasic action potential recordings (Priori *et al.* 1988; De Groot *et al.* 1995). In addition, there is paucity of evidence of correlation between myocyte spontaneous activity and the *in vivo* situation after MI.

In vivo, sympathetic imbalance and increased adrenergic drive are thought to underlie the PVCs that initiate post-MI arrhythmias, and adrenergic stimulation increases PVC incidence after MI (Rivas *et al.* 2009). After MI, cardiac innervation undergoes extensive remodelling with denervation in the scar and partial denervation and nerve re-growth or sprouting in the peri-infarct region (Cao *et al.* 2000; Rajendran *et al.* 2016). Restoring sympathetic innervation reduced post-MI arrhythmias in a recent experimental study (Gardner *et al.* 2015). Sympathetic nerve stimulation or hyperinnervation increases dispersion of repolarization resulting in arrhythmias and sudden death (Cao *et al.* 2000; Ajijola *et al.* 2017). We have previously shown that myocytes isolated from the area adjacent to MI have Ca^{2+}-driven DADs during adrenergic stimulation (Dries *et al.* 2018).

Therefore, it can be hypothesized that adrenergic stimulation leads to triggering of arrhythmias *in vivo* and, through increasing repolarization instability, contributes to the functional substrate after MI (Liu *et al.* 2015). This could remain confined to the peri-infarct region where chronic changes in local innervation may contribute to differential myocyte remodelling (Habecker *et al.* 2016; Pianca *et al.* 2019). In the present study, we have set out to investigate the above hypotheses. We study mechanisms underlying arrhythmia after MI, using adrenergic stimulation as the initiating event rather than programmed stimulation. We focus on triggers for arrhythmias and the potential for a dynamic interplay between triggers and functional substrate. Using monophasic action potential recordings, we first explore *in vivo* the regional sources of afterdepolarizations and repolarization instability and subsequently correlate these findings with intrinsic myocyte remodelling in different regions by studying the properties of isolated myocytes. Rather than noradrenaline, we use isoproterenol both for myocytes and *in vivo* experiments, to exclude α-receptor-mediated vascular effects with secondary confounding reflex activity.

Methods

Ethical approval

The animal experimental protocols used in this study were approved by the in-house ethical committee (Ethische Commissie Dierproeven, KU Leuven), with permit numbers P10139, P14176 and P16110. Animals were housed and treated according to the Guide for the Care and Use of Laboratory Animals (National Institute of Health, USA), and the European Directive 2010/63/EU; and complies with *The Journal of Physiology* ethical checklist (Grundy, 2015). A standard 14 h light, 10 h dark cycle, 22 $\pm$ 2°C temperature and 45–70% humidity was maintained. Standard chow (Optivo Pro 9041, AVEVE, Belgium) and water were provided *ad libitum* except in the days prior to and after experimental procedures when animals were either fasted or fed twice a day with welfare monitoring. All interventions were performed under full anaesthesia.

Pig model of chronic myocardial infarction

The pig model of MI was as previously described (Galan *et al.* 2016). In this model, a copper-coated stent is implanted during a percutaneous procedure. This leads to intima proliferation, severe stenosis and MI within 1 week. Twenty-seven young-adult domestic pigs (*Sus scrofa domesticus*, breed: Piétrain) of both sexes (20–25 kg) were included in the study, after a 6 week protocol. Animals were randomized to either MI ($N = 14$) or Sham ($N = 13$) groups before the stent implantation procedure on day 0.

Before coronary catherization and stent implantation, animals received amiodarone (300 mg; 3 days loading before intervention), aspirin (100 mg) and clopidogrel (300 mg; 1 day before intervention), to protect against arrhythmias and thromboembolisms during the percutaneous intracoronary intervention. Anaesthesia was induced by intramuscular injection of tiletamine/zolazepam (4 mg kg^{-1}) together with xylazine (2.5 mg kg^{-1}). Intravenous infusion of propofol (10 mg kg^{-1} h^{-1}) and remifentanil (0.018–0.03 μg^{-1} kg h^{-1}) was used for maintenance of the anaesthesia. After oral tracheal intubation, animals were mechanically ventilated with 1:1 oxygen/air. During the intervention, animals received an intravenous bolus of heparin (10000 IU) to prevent thromboembolism and were continuously monitored for heart rate and rhythm using 6-lead electrocardiogram (ECG).

For coronary catheterization and stent implantation, the right carotid artery was dissected and cannulated with an 8 Fr introducer sheath. An 8 Fr Judkins-left coronary guiding catheter was positioned in the left main coronary ostium under fluoroscopic guidance. Using a 2.5–2.75 mm angioplasty balloon, the copper-coated stent was implanted in the left anterior descending coronary artery immediately after the first diagonal branch. Sham animals underwent the same surgical procedure, without stent implantation.

After the intervention, additional analgesia and antibiotics to prevent wound infection were administered intramuscularly using buprenorphine (0.01–0.05 mg kg^{-1}) as necessary and enrofloxacin (2.5 mg kg^{-1}). Furthermore, antiplatelet medication and analgesia were orally administered on a daily basis for 6 weeks (clopidogrel (75 mg) and aspirin (100 mg) daily). Animals were monitored daily for general activity and behaviour, food intake and possible wound infections.

Table 1. Left ventricular function and remodelling after MI

	MI ($N_{pigs} = 11$)	Sham ($N_{pigs} = 9$)	*P* value
Infarct size (% of LV mass)	9.5 ± 3.5	0	<0.0001
End-diastolic volume (ml)	172 ± 31.5	132 ± 25.0	0.0059
End-systolic volume (ml)	101 ± 22.9	54 ± 11.0	<0.0001
Ejection fraction (%)	41.5 ± 5.3	58.7 ± 3.3	<0.0001
Left ventricular mass (g)	107 ± 22.0	114 ± 21.3	0.459
Left ventricular systolic pressure (mmHg)	114 ± 25.0	110 ± 15.3	0.636

As this model of MI has been previously characterized (Galan *et al.* 2016), here subsets of MI (11 out of 14) and Sham (9 out of 13) animals were used to demonstrate consistency with the established model in a structural and functional assessment using magnetic resonance imaging (MRI) 6 weeks after stent implantation (3 tesla, Magnetom PRISMA; Siemens, Erlangen, Germany). Before and during MRI, anaesthesia was induced and maintained, and animals were mechanically ventilated as described above. During imaging, heart rate and rhythm were continuously monitored using 3-lead ECG. Images were acquired using a phased-array body coil wrapped over the thorax to increase signal to noise ratio, with ECG gating. Respiration of the animal was manually stopped to reduce motion artefacts during imaging. Mechanical ventilation was again continued as soon as the collection of images was completed. All images were analysed with custom software (RightVol; KU Leuven). Infarct size was determined by late gadolinium enhancement, 12 min following a bolus of Gd (gadoterate meglumine, 0.2 mmol kg^{-1}). Table 1 summarizes the findings, confirming a mean infarct size of 10% of LV mass, with dilatation of the LV and reduced ejection fraction.

Thereafter, in the same sixth week, an *in vivo* electrophysiology study was performed.

In vivo electrophysiology study and MAP recordings

Prior to *in vivo* electrophysiological studies, anaesthesia was induced using intramuscular injection of tiletamine/zolazepam (4–8 mg kg^{-1}) only, to prevent anti-arrhythmic effects induced by xylazine (Gonca, 2015). Maintenance of anaesthesia and mechanical ventilation were performed as described above. The right and left carotid arteries, femoral artery and the femoral or jugular vein were cannulated. A bolus of heparin (5 000–10 000 IU) was periodically administered for anticoagulation. Under fluoroscopic guidance, monophasic action potential (MAP) catheters (MedFact GmbH, Germany) were inserted into the LV and positioned in the peri-infarct and non-infarcted remote region, guided by fluoroscopy and coronary angiography and the absence of a MAP signal in the infarct area (Fig. 1*A*). A 7 Fr diagnostic electrophysiology catheter (Biosense Webster, Belgium) was positioned in the right atrium for pacing. Continuous 12-lead ECG and simultaneous MAPs in both peri-infarct and remote regions were recorded at 4 kHz using a Labsystem Pro EP recording system (Boston Scientific, USA). To eliminate effects of heart rate variations, animals were atrially paced at 120 beats min^{-1}, and recordings were performed at baseline pacing and during pacing with infusion with isoproterenol (ISO; 1–2 µg min^{-1}; Isuprel). This dose was chosen based on its use clinically to facilitate arrhythmia testing (Heidbüchel *et al.* 2003) and to provoke afterdepolarizations in at-risk patients (Shimizu *et al.* 1991). Following the experiments, animals received the same care as described above.

At baseline, the following acceptance criteria for MAP recordings was applied: amplitude of at least 10 mV, with an identifiable plateau, and a stable baseline (Franz, 1999). DADs were defined as an increase in baseline potential exceeding 1 mV in amplitude. DAD incidence and amplitude were analysed; DAD amplitude was normalized to the amplitude of the precedent AP. Beat-to-beat variability of repolarization (BVR), a marker of repolarization instability, was calculated as short-term variability of 90% of MAP duration ($MAPD_{90}$) from 30 consecutive APs by:

$$\Sigma(|MAPD_{90_{i+1}} - MAPD_{90_i}|) / [n \text{ beats} \times \sqrt{2}]$$

(Thomsen *et al.* 2004);

Only paced beats were taken into account. During a 5-min period after stabilization and ISO infusion, ventricular extrasystoles or arrhythmias were quantified and reported as events per minute. Arrhythmic events were also translated into a score, accumulating all events over the 5-min recording.

Cell isolation

After 3–5 days recovery from the *in vivo* studies, animals were euthanized. Anaesthesia was induced as described above and maintained using intravenous administration

of pentobarbital (2.5 mg kg^{-1}), while mechanically ventilating the animals. Thereafter, the thorax was quickly opened, an overdose of pentobarbital (20 mg kg^{-1}) was given and the heart was taken out. Biopsies were taken for molecular studies and hearts processed for cellular studies. Single cardiomyocytes from the LV were enzymatically isolated from the peri-infarct region and non-infarcted remote region in MI pigs, and from matching regions in Sham pigs (Nagaraju *et al.* 2017). The coronary artery perfusing these regions was cannulated and a wedge of tissue excised and enzymatically digested on a constant flow perfusion system at 37°C. The digested tissue was minced and filtered, and the isolated myocytes resuspended in HEPES-buffered Tyrode solution (in mmol l^{-1}: NaCl 137, KCl 5.4, $MgCl_2$ 0.5, $CaCl_2$ 1.8, Na-HEPES 11.8, and glucose 10; pH 7.4). After isolation, the cells were allowed to recover for 1 h before experiments were commenced.

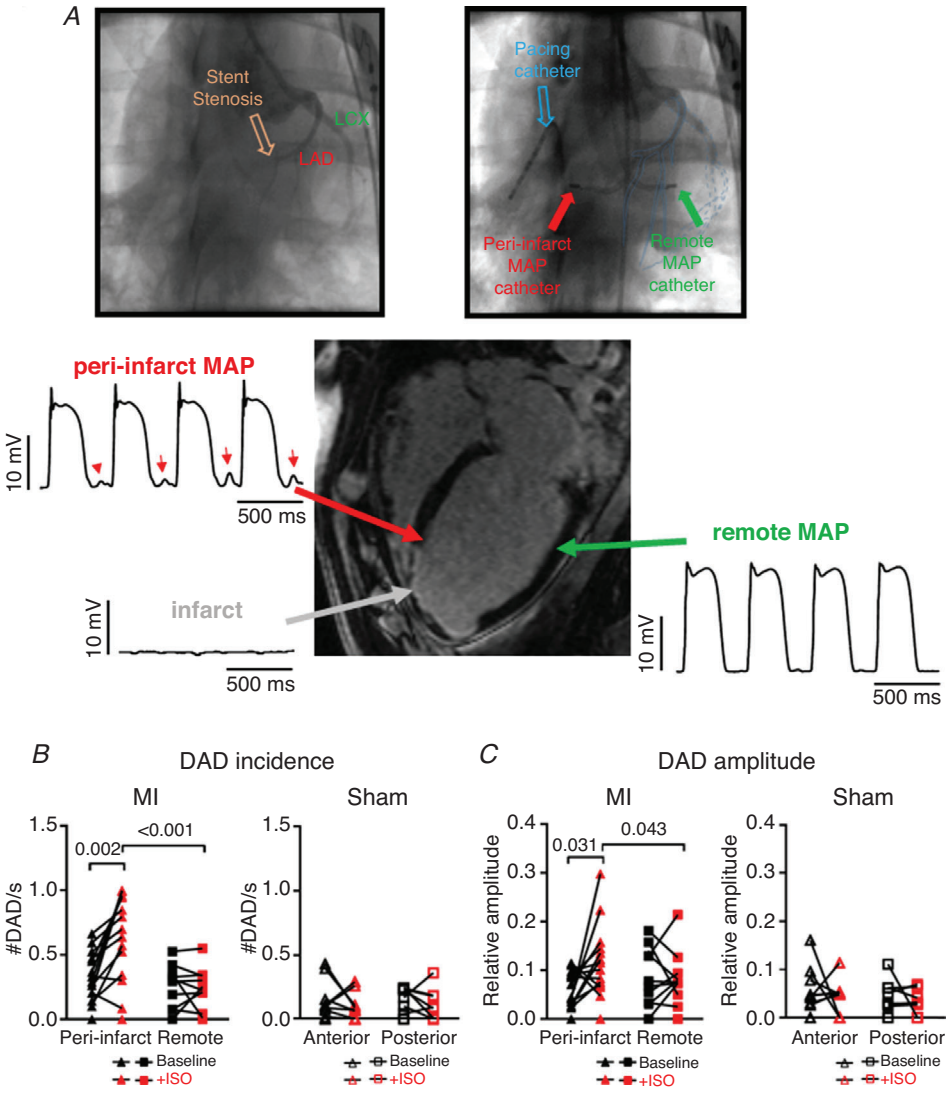

Figure 1. *In vivo* adrenergic stimulation induces more and higher amplitude delayed afterdepolarizations (DADs) in the peri-infarct region
A, example of data acquisition in an MI pig with regional catheter positioning guided by coronary angiography and absence of monophasic action potential (MAP) in the infarct. Top left: coronary angiography with stenosis indicated by the arrow (LAD, left anterior descending coronary artery; LCX, left circumflex coronary artery). Top right: overlay of the coronary angiography and positioning of the MAP catheters in the peri-infarct and remote regions and pacing catheter in the right atrium. Bottom: pre-procedural MRI illustrating the infarct, peri-infarct and remote regions with corresponding examples of *in vivo* regional MAP recordings during ISO infusion (red arrows illustrate DADs in the peri-infarct region). *B* and *C*, mean data for DAD incidence (*B*) and amplitude (*C*) in MI (N_{pigs} = 14) and Sham (N_{pigs} = 10) animals. Repeated measures two-way ANOVA with Bonferroni *post hoc* testing.

Cell structure measurements

Cell size (length and width) was measured in randomly selected cells from both regions of Sham and MI. Sarcolemma, transverse and axial tubular structures (TATS) were stained by incubating cells with Alexa Fluor 594 conjugated to wheat germ agglutinin (WGA, 10 μg ml^{-1}; ThermoFischer, W11262). Images were collected in a *Z*-stack using a 40× objective, 1.3 NA oil immersion, on a Zeiss LSM 510 confocal microscope and quantified using Image J software (NIH, USA, v1.5, RRID: SCR_003070). TATS signals within the cell margins were identified against the background by thresholding. The sarcolemmal membrane was subtracted from thresholded images. Thresholded images were further processed to skeletonize TATS signals. TATS density was quantified as the number of signal-positive pixels over all pixels within the cell margins.

Cellular electrophysiological and calcium recordings

Cells were studied in whole-cell patch clamp mode, using either voltage- or current-clamp configuration (Axon 200B amplifier, Axon Instruments). Cells were constantly superfused with HEPES-buffered Tyrode solution at 37°C and patch pipettes (2–3 MΩ) (GB 200-8P, Science Products) were filled with (in mmol l^{-1}): potassium aspartate 120, NaCl 10, KCl 20, K-HEPES 10, MgATP 5, and K_5Fluo-4 0.05; pH 7.2. In voltage-clamp mode, cells were stimulated for 2 min using 200 ms depolarizing steps from −70 mV to +10 mV at 2 Hz stimulation frequency and with recording for 15 s at −70 mV after stopping stimulation. In current-clamp mode, cells were stimulated with a suprathreshold depolarizing pulse of 2–5 nA, at 2 Hz and 1 Hz for 3–5 min in steady states. In both modes, Ca^{2+} was simultaneously recorded. Ca^{2+} transients were recorded on a photometry epifluorescence set-up, with $[Ca^{2+}]_i$ reported as the fluorescence normalized to baseline values, after background subtraction as F/F_0. In other experiments, local Ca^{2+} events (Ca^{2+} waves, Ca^{2+} sparks) and Ca^{2+} transients (used for kinetic measurements) were recorded using confocal line-scanning along the long axis of the cell in a central plane and avoiding the nucleus (Zeiss LSM 510, 40× oil immersion objective; scanning at 650 Hz with a pixel size of 0.2–0.3 μm). Ca^{2+} waves were recorded as previously described and quantified using a custom-made analysis program (Dries *et al.* 2018). Ca^{2+} wave incidence was normalized to cell length and time as number of waves 100 μm^{-1} s^{-1}. We defined coupled (dyadic) and non-coupled (non-dyadic) release sites as previously described (Dries *et al.* 2018). SR Ca^{2+} content was measured by integrating the inward NCX current (I_{NCX}) during rapid caffeine superfusion (10 mmol l^{-1} for 8 s) after a conditioning train of 2 Hz stimulation. AP duration was calculated at APD_{90} and BVR was calculated as described above. All protocols were performed at baseline and presence of 10 nM ISO, a low concentration chosen to detect increased sensitivity.

Quantitative real time PCR experiments

After harvesting the heart, peri-infarct and remote tissue samples from MI and matched anterior and posterior regions in Sham were snap-frozen in liquid nitrogen and immediately stored at −80°C. Total RNA was extracted from all frozen biopsies with an miRNeasy mini kit according to the manufacturer's instructions (Qiagen, Hilden, Germany). A 500 ng sample of total RNA was used for cDNA synthesis with SuperScript II Reverse Transcriptase (Thermo Fisher Scientific, Carlsbad, USA). The final cDNA concentration was 1.25 ng μl^{-1}.

mRNA levels of genes encoding calcium handling proteins, ion channels and adrenergic signalling components were measured by real-time qRT-PCR using gene specific primers (Table 2) and GoTaq qPCR Master Mix (Promega, Madison, USA). Amplification was performed using a CFX384 Real-Time PCR Detection System. Results are presented as relative mRNA abundance, with each sample normalized to the geometric mean of RPL32 and TBP, which were used as reference genes. The stability of these reference genes was first established using geNORM (Vandesompele *et al.* 2002).

Western blot for protein expression

Snap frozen samples of regional myocardial tissue were homogenized in a buffer containing (in mM): imidazole 10, sucrose 300, dithiotreitol 1, sodium metabisulfite 1, sodium fluoride 25, sodium ethylene diaminetetraacetic acid (EDTA) 5, sodium pyrophosphate 5, phenylmethylsulfonyl fluoride 0.3, and a protease inhibitor cocktail ('Complete-Mini' Roche Molecular Biochemicals). Equal amounts of proteins were then separated on a 4–12% Bis-Tri gradient gel (Invitrogen) and transferred onto polyvinylidene difluoride membrane (Millipore). The membrane was blocked with Odyssey TBS blocking buffer. Blocked membranes were then incubated with antibodies for CaMKII (1:1000 dilution, SC-5392, Santa Cruz) and GAPDH (1:10,000 dilution, G8795, Sigma) overnight at 4°C. Detection was performed using IRDye secondary antibodies (1/15,000 dilution, LI-COR) and blots were scanned using an infrared imaging system (Odyssey CLx, LI-COR); in Fig. 10 the full-length blots are shown. Band intensity was quantitated using Image Studio software. The membrane was stripped with antibody stripping solution (2504, Millipore) and re-probed with the Phospho-CaM Kinase II pThr286 antibody (PA1-14076, Invitrogen). The detection was performed again using IRDye secondary antibody. The band intensity was analysed using Image Studio software.

Table 2. PCR Primers

Gene product	Gene name	Forward primers (5′-3′)	Reverse primers (5′-3′)
Inward rectifier potassium channel	KCNJ2	CCGCTACAGCATTGTCTCTT	TGGACCTTACTCTTCCCGTT
Delayed rectifier (rapid) potassium channel	KCNH2	TGGGCTTTGGCAATGTCTC	AAGATGCTGGCGTACATGAG
Delayed rectifier (slow) potassium channel	KCNQ1	CTGGAAGTGCTTCGTCTACC	GCGACATACTGCTCAATGGT
Natriuretic peptide A	NPPA	CTTCGGGGGTAGGATGGACA	TCTTCAGTACCGGAAGCTGTTA
β_1-Adrenergic receptor	β_1AR	CCAACCTCTTCATCATGTCC	GCAGAAGAAGGAGCCGTACT
B_2-Adrenergic receptor	β_2AR	CCAGACGGTCACCAACTACT	CCGAAAGTCCACATTTTCAT
G protein-coupled receptor kinase 2	GRK2	ATGCAGAAGTACCTGGAGGA	ACAGAAGTCTCGGAAAAGCA

Experimental design and statistics

Data acquisition was performed by multiple investigators. Investigators were blinded when doing analysis off-line by creating coded data files. For quality control and to check on consistency, sets of experiments were analysed by two independent and blinded investigators.

All individual data points are shown in dot plots, with each dot representing the data of an animal. In the case of cellular studies with multiple cells per animal, the dot plot is the mean value for this animal. Statistically, data were compared using a nested design taking into account the number of cells (n) and animals (N), with Student's t test or a two-way ANOVA with Bonferroni *post hoc* testing; repeated measures was used when the same samples were measured before and after ISO treatment. A chi-squared test was used to compare proportions. In one data set we examined correlations using regression analysis, linear fitting and two-tailed t test. Data were considered significantly different when the P value was < 0.05, while the exact values have been inserted in the graphs. Additional information on statistical testing may be found online in the Statistical Summary Document.

Results

Increased incidence and amplitude of DADs in the peri-infarct region *in vivo*

Figure 1*A* illustrates MAPs simultaneously recorded in the MI peri-infarct and remote region during atrial pacing at 2 Hz. At baseline, there was no difference in DAD incidence or amplitude between regions in either Sham or MI. However, during ISO infusion, there was both an increased incidence and amplitude of DADs in the MI peri-infarct region compared to baseline and to the MI remote region (Fig. 1*B* and *C*). Infusion of ISO did not alter the DAD incidence or amplitude in the corresponding regions in Sham animals.

BVR is larger in the peri-infarct than remote region *in vivo*

We also examined repolarization properties that could facilitate arrhythmia by analysing AP duration and BVR (Fig. 2*A*). During 2 Hz atrial pacing, the mean MAP duration (MAPD) was not different between the MI peri-infarct and remote regions and was also not different compared to matched Sham regions at baseline and during ISO (data not shown). There were no apparent regional differences in BVR of MAPD in either MI or Sham animals at baseline. During ISO infusion, BVR increased significantly in both the peri-infarct and remote regions but eventual BVR was significantly larger in the peri-infarct region than in the remote region (Fig. 2*B*).

More PVCs and complex extrasystoles during ISO *in vivo*

The peri-infarct increase in DADs and BVR during ISO resulted in a higher arrhythmia potential in MI pigs, as recorded in the ECG. Occasionally a local peri-infarct DAD appeared to precede a PVC on the ECG (Fig. 3*A*), though a causal relation could not be ascertained. MI pigs had a higher incidence of PVCs per minute compared to Sham animals (Fig. 3*B*). Additionally, more couplets (two consecutive beats; $p = 0.095$), triplet PVCs (three consecutive beats; $p = 0.014$) and non-sustained ventricular tachycardia (VT) ($p = 0.028$) were observed in MI pigs during ISO, compared to Sham animals, translating into a higher arrhythmia score after MI (Fig. 3*C*).

Cellular hypertrophy and altered Ca^{2+} handling in peri-infarct and remote myocytes

We postulated that the regional arrhythmic potential in the peri-infarct region was related to a more pronounced cellular remodelling. To investigate this possibility, we isolated and compared the phenotypes and physiology of cardiomyocytes from the different study regions (Fig. 4*A*). In both MI peri-infarct and remote myocytes, cell width and length were significantly increased and density of the transverse and axial tubular structures (TATS) was reduced compared to Sham myocytes (Fig. 4*B*). Baseline Ca^{2+} transients from both MI peri-infarct and remote myocytes were reduced in amplitude and rate of upstroke compared to Sham myocytes (Fig. 4*C*), without differences

in the SR Ca^{2+} content (data not shown). Concurrent with reduced TATS density, the distribution of the time to half-maximal Ca^{2+} release was shifted to the right, with more delayed sites in MI myocytes (Fig. 5*A*). Sites defined as non-coupled were more numerous in MI (Fig. 5*B*).

These data indicate that after MI, structural and functional myocyte remodelling occurs throughout the whole LV.

Higher prevalence of Ca^{2+} waves, DADs and spontaneous APs in peri-infarct myocytes in the presence of ISO

To relate myocyte function to the *in vivo* observations, we assessed the arrhythmic potential of cells under ISO. To this end, we applied a conditioning train of square depolarizing pulses at 2 Hz and subsequently measured spontaneous Ca^{2+} releases and corresponding membrane currents. Spontaneous releases were seen in all groups, but MI peri-infarct myocytes had a significantly higher frequency of Ca^{2+} waves and depolarizing currents compared to MI remote and Sham myocytes (Fig. 6*A*). This translated into more DADs as well as spontaneous APs in current clamp mode (Fig. 6*B*).

Inhibition of CaMKII signalling using autocamtide-2 related inhibitory peptide (AIP, 10 μM), a highly specific CaMKII inhibitor, was able to lower the incidence of DADs in MI peri-infarct myocytes (Fig. 6*C*).

Increased BVR in MI peri-infarct myocytes in the presence of ISO

We further investigated cellular AP repolarization and BVR under current-clamp conditions, to compare with the *in vivo* observations during 2 Hz atrial pacing. However, 48% of MI peri-infarct myocytes had impaired frequency-dependent acceleration of repolarization and did not follow 2 Hz pacing because of incomplete

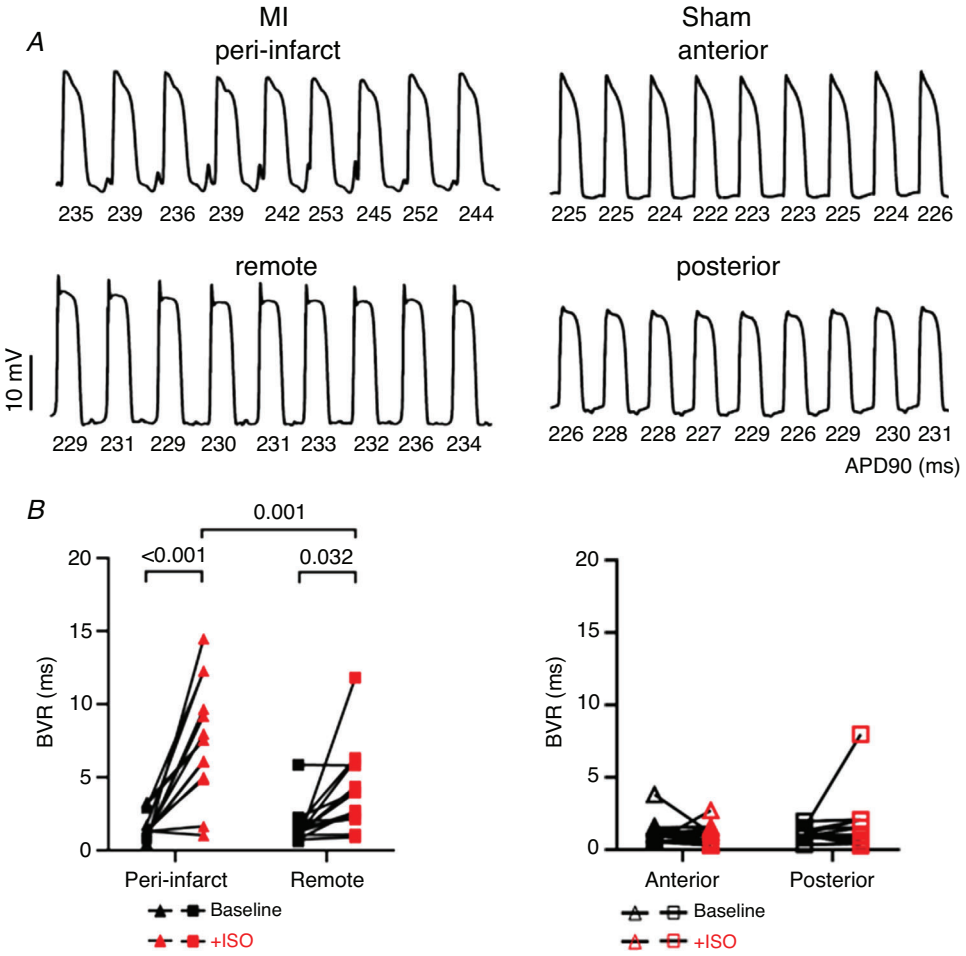

Figure 2. Adrenergic stimulation induces higher beat-to-beat variability of repolarization (BVR) in the peri-infarct region *in vivo*
A, examples of BVR during ISO infusion *in vivo*: MAP recordings in MI peri-infarct and remote regions and matched Sham anterior and posterior regions. *B*, mean data for regional BVR in MI (N_{pigs} = 14) and Sham (N_{pigs} = 13) animals. Repeated measures two-way ANOVA with Bonferroni *post hoc* testing.

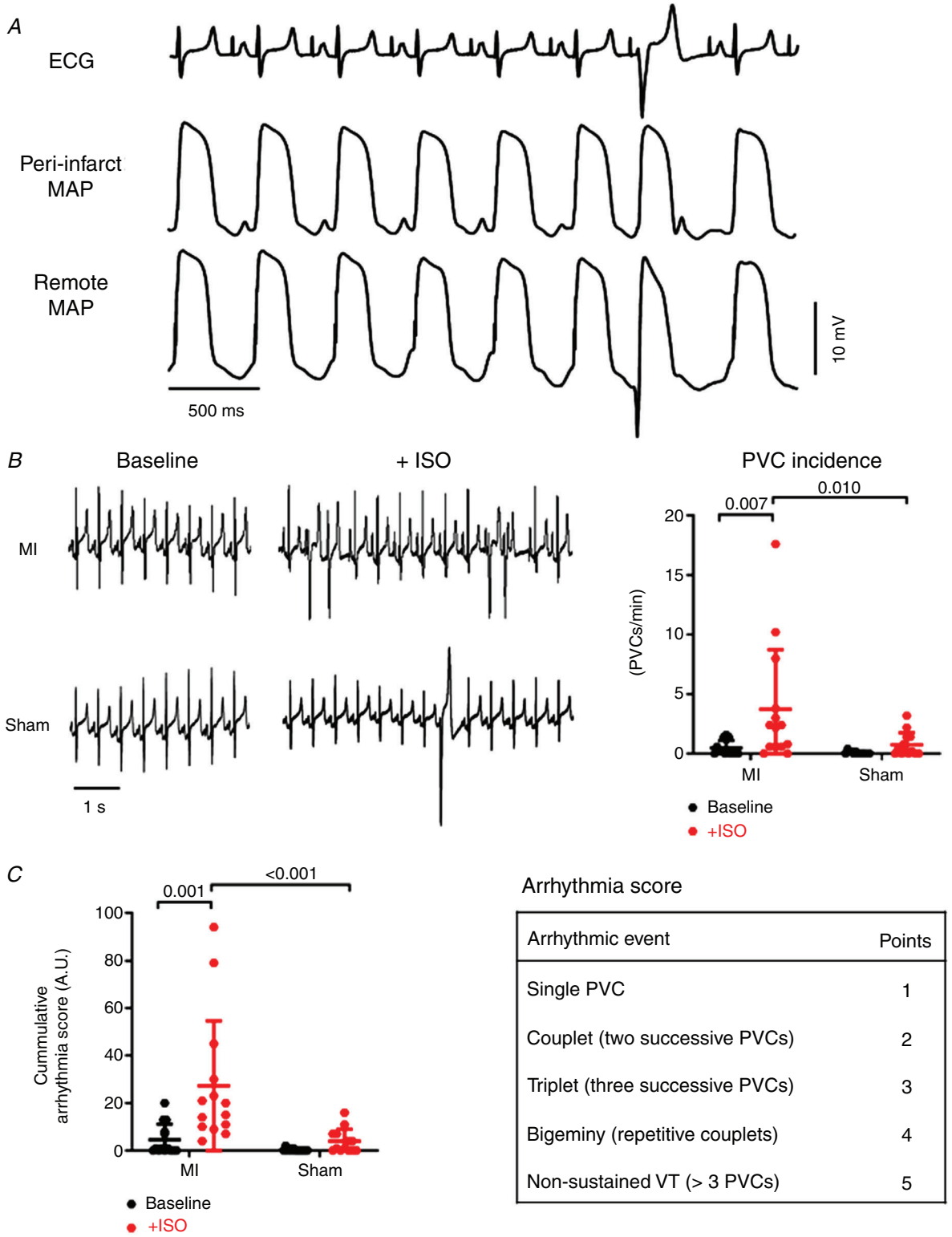

Arrhythmia score

Arrhythmic event	Points
Single PVC	1
Couplet (two successive PVCs)	2
Triplet (three successive PVCs)	3
Bigeminy (repetitive couplets)	4
Non-sustained VT (> 3 PVCs)	5

Figure 3. PVCs and arrhythmias in MI pigs during ISO infusion
A, example of DADs in the peri-infarct region with a PVC on ECG. *B*, examples of ECG in MI and Sham pigs before and after infusion of ISO with mean data for PVC incidence. *C*, arrhythmia scoring using criteria in the table on the right. Data from MI (N_{pigs} = 14) and Sham (N_{pigs} = 13) animals before and after ISO infusion. DAD, delayed afterdepolarization; PVC, premature ventricular complex. Repeated measures two-way ANOVA with Bonferroni *post hoc* testing.

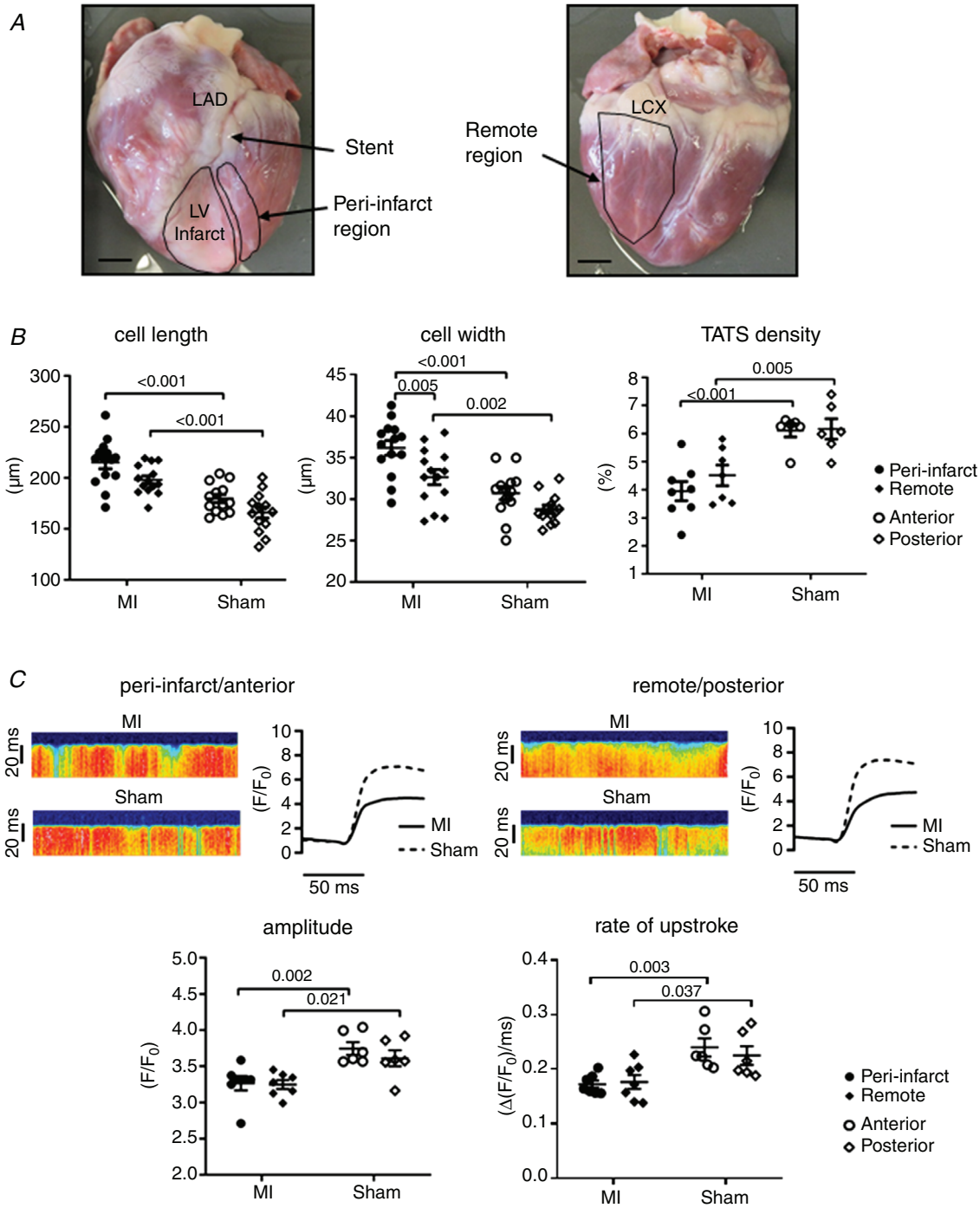

Figure 4. Regional myocyte remodelling and Ca^{2+} handling after MI
A, photographs of an infarcted heart showing the peri-infarct and remote regions used for cell isolation. Scale bar, 1 cm; LV, left ventricle; LAD, left anterior descending coronary artery; LCX, left circumflex coronary artery. *B*, mean data for cell size (MI: n_{cells} = 178–192; N_{pigs} = 14; Sham: n_{cells} = 164–218; N_{pigs} = 13) and TATS density (MI: n_{cells} = 24–27; N_{pigs} = 7–8; Sham: n_{cells} = 18–21; N_{pigs} = 6) in different regions of MI and Sham myocytes. *C*, top: example of confocal line scan recording of Ca^{2+} transient and corresponding plots in different regions for MI and Sham myocytes. Bottom, mean data for Ca^{2+} transient amplitude and rate of upstroke in different regions for MI (n_{cells} = 24–27; N_{pigs} = 7) and Sham (n_{cells} = 17–18; N_{pigs} = 6) myocytes. Two-way ANOVA with Bonferroni *post hoc* testing.

repolarization within 500 ms, compared to 20% in MI remote myocytes ($p = 0.002$) and to 13% in the corresponding Sham region ($p < 0.0001$). In order not to exclude a large fraction of cells, the effects of ISO on AP repolarization were studied during 1 Hz stimulation. Under ISO, APD shortened to a greater extent in Sham myocytes when compared to MI myocytes, resulting in peri-infarct myocytes displaying a significantly longer APD_{90} than Sham in the presence of ISO (351 ± 12 ms *vs.* Sham: 223 ± 10 ms, $p = 0.002$).

Under ISO, BVR was increased significantly in the MI peri-infarct myocytes compared to MI remote myocytes and occasionally early afterdepolarizations (EAD) were observed (Fig. 7*A*). In Sham myocytes, BVR did not increase significantly with ISO (Fig. 7*B*).

Taken together, these data indicate that the peri-infarct myocytes have reduced repolarization reserve and a higher degree of instability, further exacerbated under ISO, than myocytes from the remote region, or from Sham.

Spontaneous Ca^{2+} waves and DADs contribute to BVR

We further examined the interplay between the occurrence of spontaneous Ca^{2+} release, DADs and BVR. After a Ca^{2+} wave and accompanying DAD, the Ca^{2+} transient during the stimulated AP merged with the wave and was

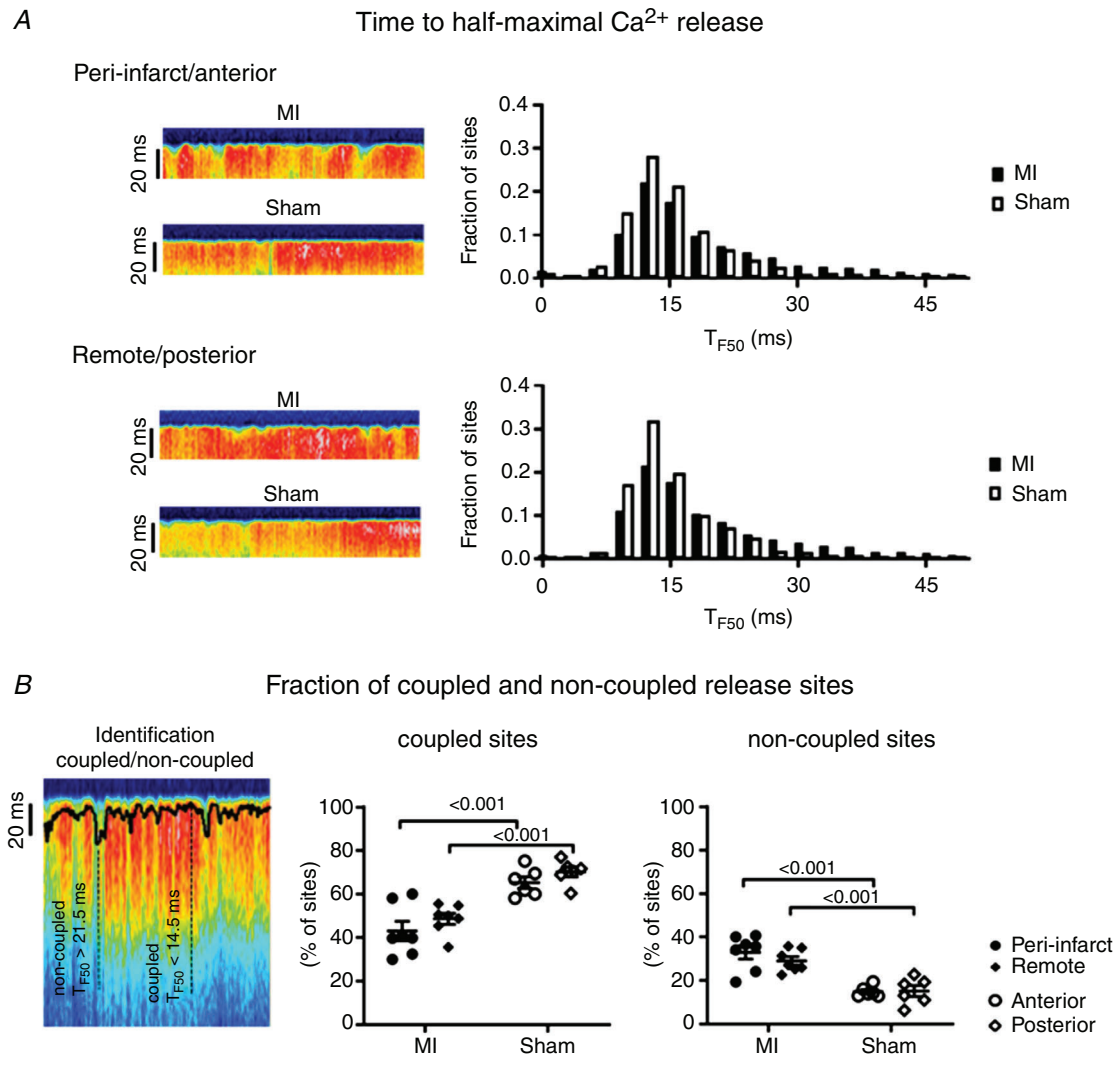

Figure 5. Delayed Ca^{2+} release in myocytes from both peri-infarct and remote regions
A, examples of confocal line scan images and distribution plots of the time to half-maximal Ca^{2+} release of the Ca^{2+} transient (T_{F50}) of Ca^{2+} release along line scans in MI ($n_{cells} = 26–27$; $N_{pigs} = 7$) and Sham ($n_{cells} = 17–18$; $N_{pigs} = 6$) myocytes from peri-infarct/anterior and remote/posterior regions. *B*, left: example of a confocal line scan image with the use of cut-off criteria for time to half-maximal Ca^{2+} release of the Ca^{2+} transient (T_{F50}) to identify coupled and non-coupled Ca^{2+} release sites. Right: mean data from coupled and non-coupled sites in MI ($n_{cells} = 26–27$; $N_{pigs} = 7$) and Sham ($n_{cells} = 17–18$; $N_{pigs} = 6$) myocytes in different regions of the heart. Two-way ANOVA with Bonferroni *post hoc* testing.

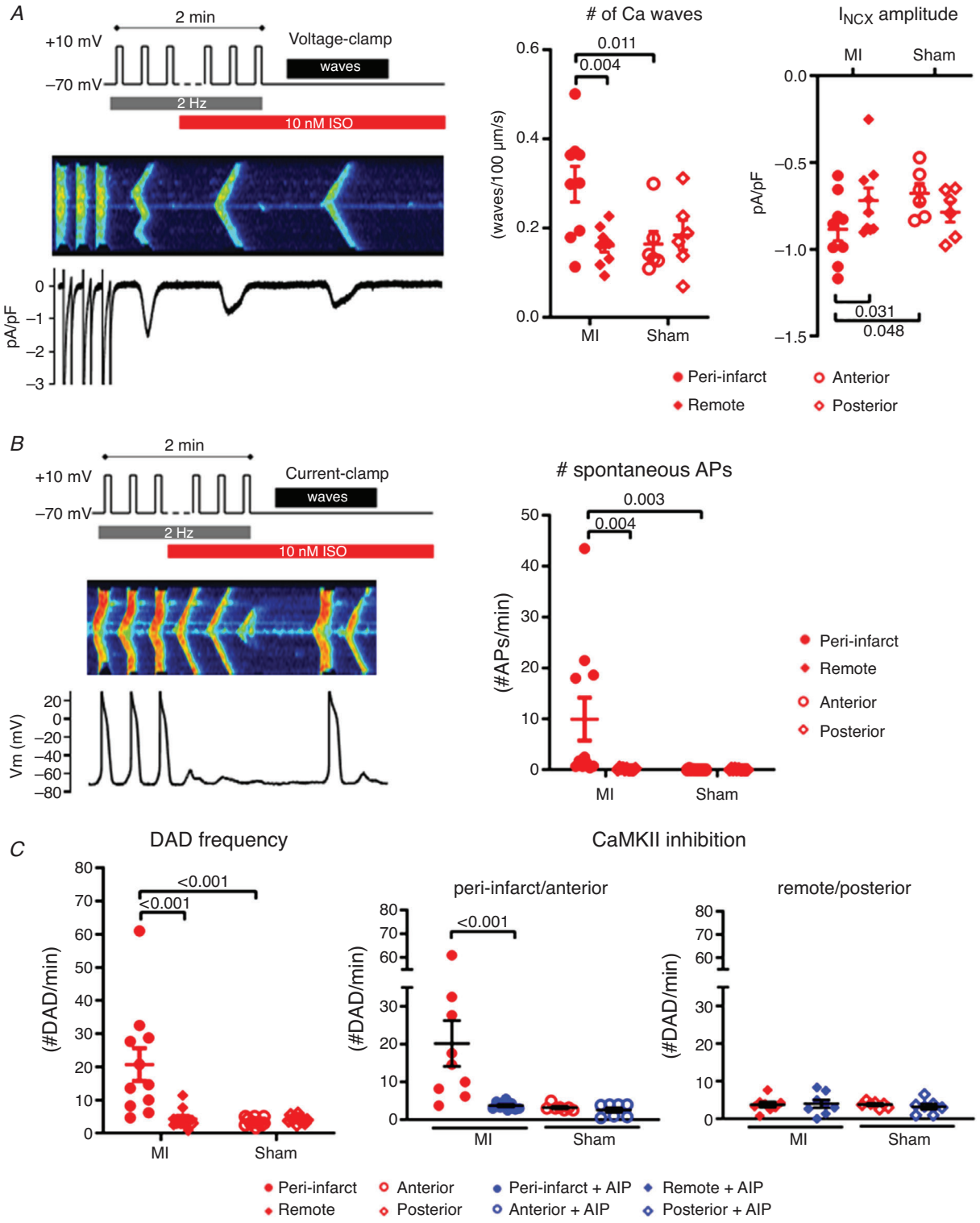

Figure 6. More Ca^{2+} waves and DADs in peri-infarct myocytes under ISO
A, left: example and protocol under voltage clamp. Right: mean data for Ca^{2+} waves and NCX currents in different regions in MI (n_{cells} = 44–46; N_{pigs} = 9) and Sham (n_{cells} = 24–27; N_{pigs} = 6) myocytes. *B*, left: example and protocol with switch to current clamp. Right: mean data for DAD frequency and spontaneous APs in different regions in MI (n_{cells} = 36–57; N_{pigs} = 11) and Sham (n_{cells} = 48–52; N_{pigs} = 11) myocytes. *C*, mean data for DAD frequency in the presence and absence of the specific CaMKII inhibitor (AIP) in MI (−AIP: n_{cells} = 20–46; N_{pigs} = 9; +AIP: n_{cells} = 22–31; N_{pigs} = 9) and Sham (−AIP: n_{cells} = 16–18; N_{pigs} = 7; +AIP: n_{cells} = 22–30; N_{pigs} = 7) myocytes from different regions of the heart. Two-way ANOVA with Bonferroni *post hoc* testing.

generally smaller. As illustrated in Fig. 8*A*, this stimulated AP following a DAD with a Ca wave (marked with an arrow) was longer than the preceding AP. Analysis of the grouped data confirmed that in MI, higher DAD incidence, associated with Ca^{2+} waves, correlated with higher BVR, with the incidence of both DADs and BVR highest in peri-infarct myocytes (Fig. 8*B*).

Molecular actors in adrenergic signalling show regional differences in their expression

In tissue samples, we examined regional expression levels of a panel of genes selected based on their relation to the functional observations. Of the genes encoding major K^+ channels in pig heart (which lacks transient outward K^+ channels), only *KCNJ2*, encoding the channel for the inward rectifier current I_{K1}, was reduced significantly in the peri-infarct region (Fig. 9*A*). The expression of *ADRB1*, coding for β_1-adrenergic receptor was significantly reduced in the MI peri-infarct region compared to MI remote region (Fig. 9*B*). Expression of *NPPA*, as a marker for hypertrophy, was larger in the peri-infarct region than in the remote region (Fig. 9*C*).

We expanded the study of cellular adrenergic signalling examining the expression of CaMKII and constitutive phosphorylation in tissue biopsies but could not find any differences (Fig. 10*A*). In a pilot experiment, we compared the effect of β_1 and of β_2 block on Ca^{2+} transients and sparks recorded in the presence of ISO, in isolated myocytes from the peri-infarct region and matching Sham

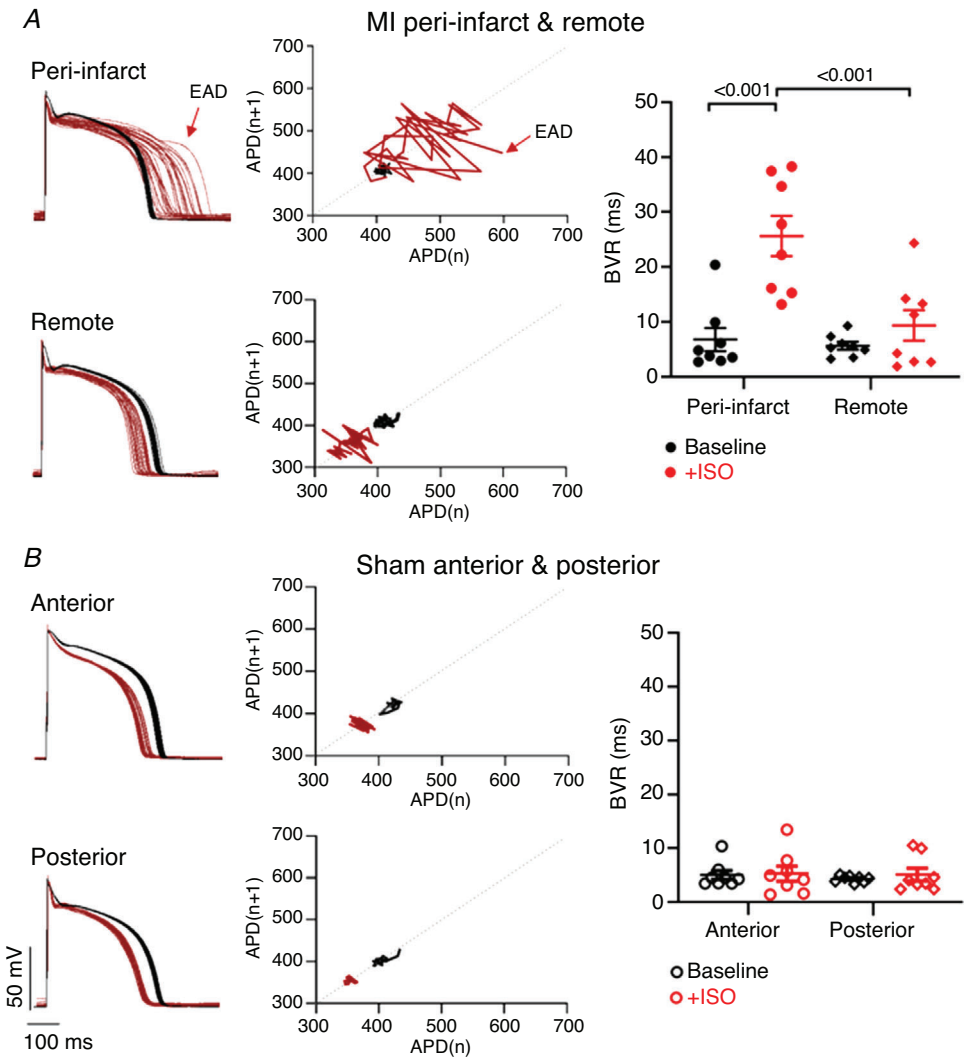

Figure 7. Higher BVR in peri-infarct myocytes under ISO
A and *B*, left: examples of 30 steady state action potentials at baseline (black) and under ISO (red); middle: their corresponding Poincaré plots of myocytes from the different regions for MI (*A*) and Sham (*B*) myocytes. Right: mean data for cellular BVR in different regions for MI (n_{cells} = 39–46; N_{pigs} = 8) and Sham (n_{cells} = 40–42; N_{pigs} = 8) myocytes. Repeated measures two-way ANOVA with Bonferroni *post hoc* testing.

region (Fig. 10*B*). MI myocytes had a response to β_2 block and less to β_1 block.

Discussion

The main findings of this study are that *in vivo*, under adrenergic stimulation with ISO, the peri-infarct, but not the remote, region is a source of triggered activity and of repolarization instability creating a functional substrate for re-entry. This is related to intrinsic myocyte properties. While myocytes from both peri-infarct and remote regions share features of remodelling, other properties are unique to the peri-infarct region, in particular the adrenergic response.

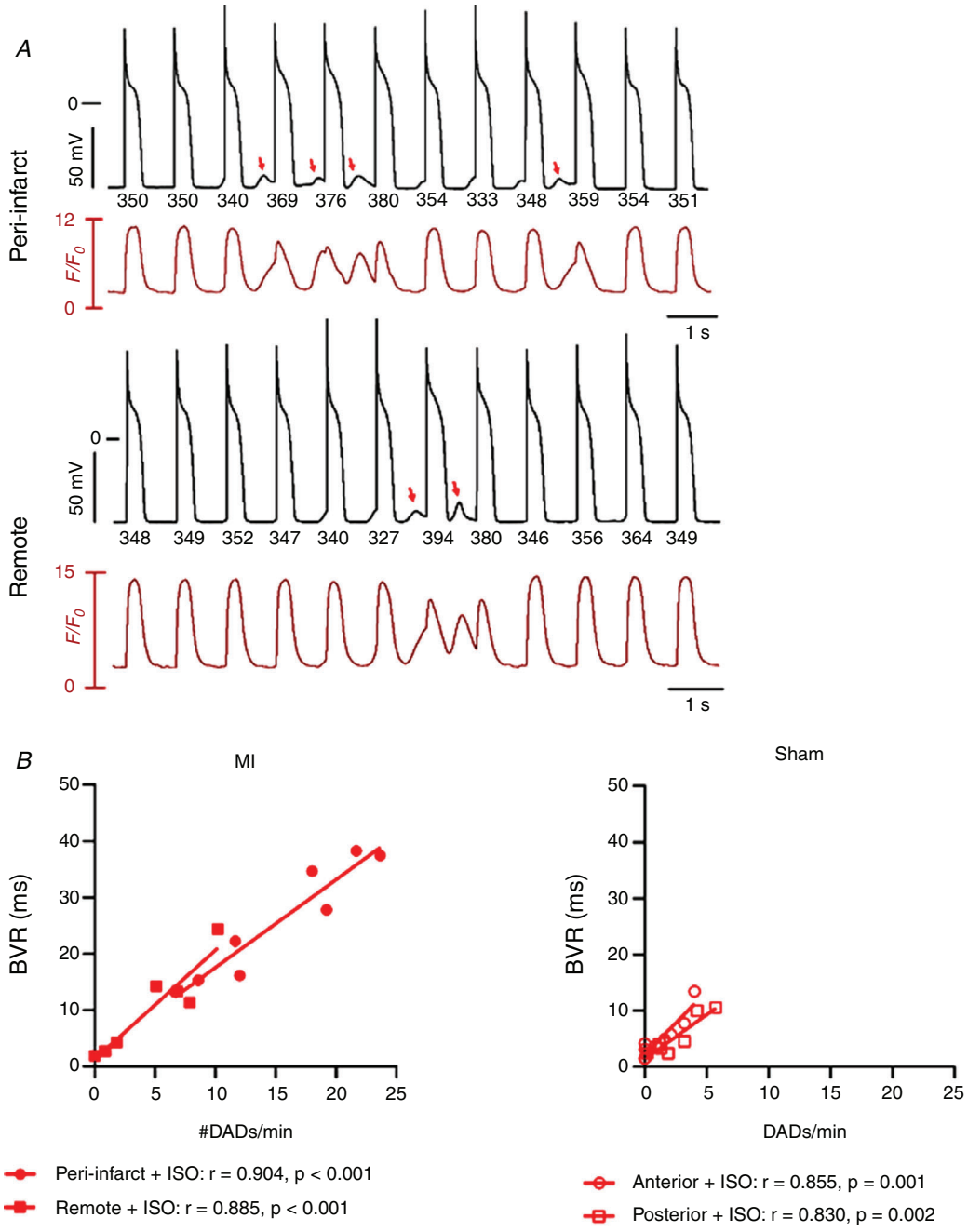

Figure 8. Spontaneous Ca^{2+} release and DADs are associated with increased BVR in peri-infarct myocytes
A, examples illustrating spontaneous Ca^{2+} release DAD contributing to subsequent Ca^{2+} transient and action potential duration (APD) changes. Red arrows indicate stimulated AP with merger Ca events and longer APD. *B*, correlation between DADs and BVR in myocytes from the different regions of MI (n_{cells} = 14–23; N_{pigs} = 8) and Sham (n_{cells} = 6–8; N_{pigs} = 6). Linear regression fitting and correlation analysis with two-tailed *t* test.

The peri-infarct region as source of triggered activity and repolarization instability *in vivo*

Studies of ventricular arrhythmia using programmed electrical stimulation identify vulnerable substrates and sources of PVCs, but cannot distinguish whether the latter result from triggered activity or (micro) re-entry. Here we used MAP catheters to study local events and thereby regional differences in repolarization and after-depolarizations, and this in the absence of programmed electrical stimulation. The MAP recording reflects the myocyte transmembrane action potential, even if reporting from groups of cells rather than a single cell. Thereby it provides a view of myocyte behaviour *in vivo*, and is a highly valuable tool to demonstrate the presence of early and delayed afterdepolarizations *in vivo*, including in clinical studies (Moore & Franz, 2007). In the pig post-MI, DADs were mostly observed in the peri-infarct region, and this observation correlated with unique properties of the myocytes isolated from this region.

These data extend findings from previous studies by Boyden and colleagues that identified Purkinje fibres as a potential source of PVCs in the first days after MI. Isolated Purkinje cells and tissues have abnormal calcium handling and DADs (Hirose *et al.* 2008). Electrical remodelling of Na^+ channels can further facilitate arrhythmias *in vivo* through altered conduction, with a potential role for oxidized CaMKII (Christensen *et al.* 2009; Dun *et al.* 2013, 2018). Recently, Hegyi *et al.* (2018) studied isolated myocytes from the post-MI pig heart, but without prior matched *in vivo* recordings. They reported more DADs and spontaneous APs in myocytes isolated from the MI border zone compared to the remote zone without adrenergic stimulation. We did not see such differences at baseline in

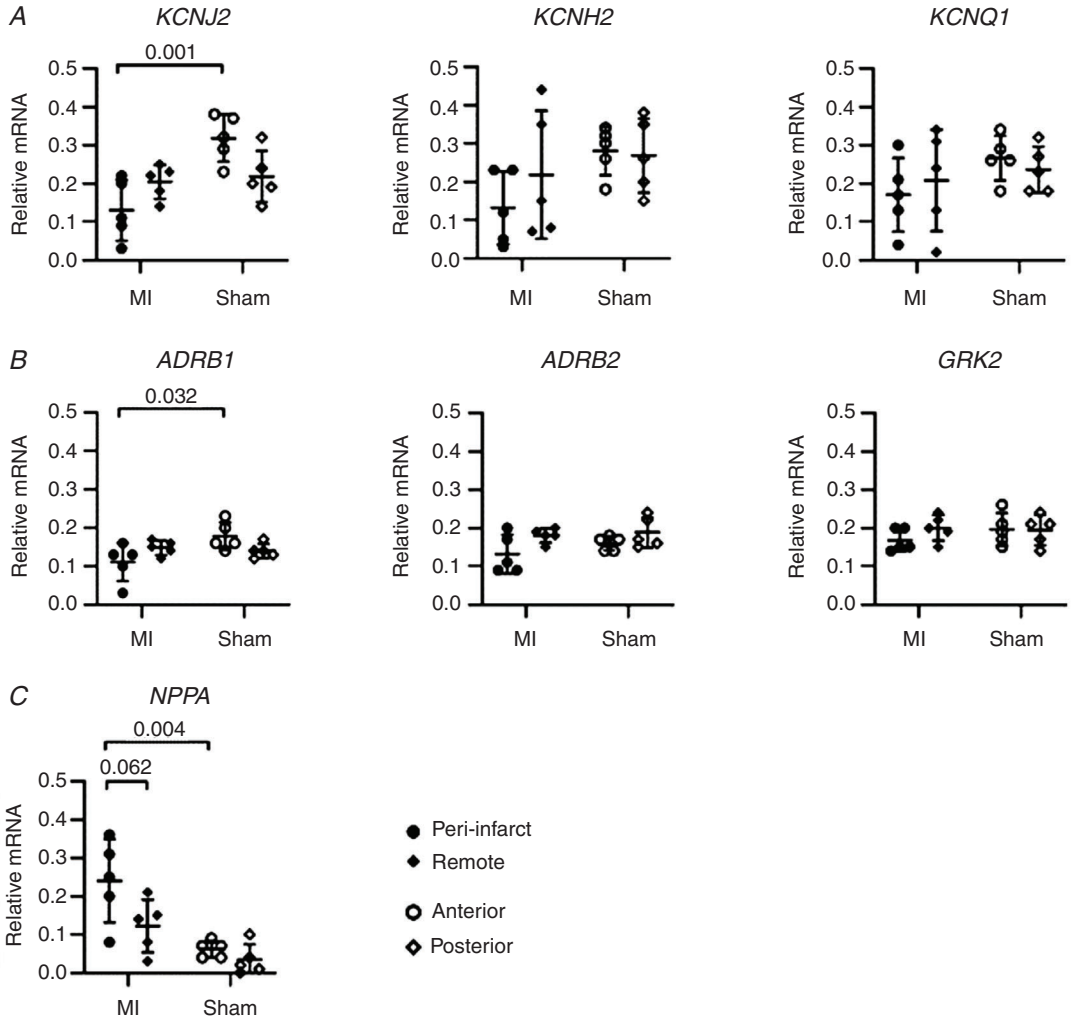

Figure 9. Post-MI differences in gene expression
A, reduced expression of *KCNJ2* coding for the inward rectifier current, I_{K1}, in the MI peri-infarct region. *B*, β-adrenergic receptor 1:2 stoichiometry shifted with reduced β_1 receptor transcription. *C*, increased transcription of a hypertrophic marker gene, natriuretic peptide A (*NPPA*) in MI (N_{pigs} = 5) and Sham (N_{pigs} = 5). Two-way ANOVA with Bonferroni *post hoc* testing.

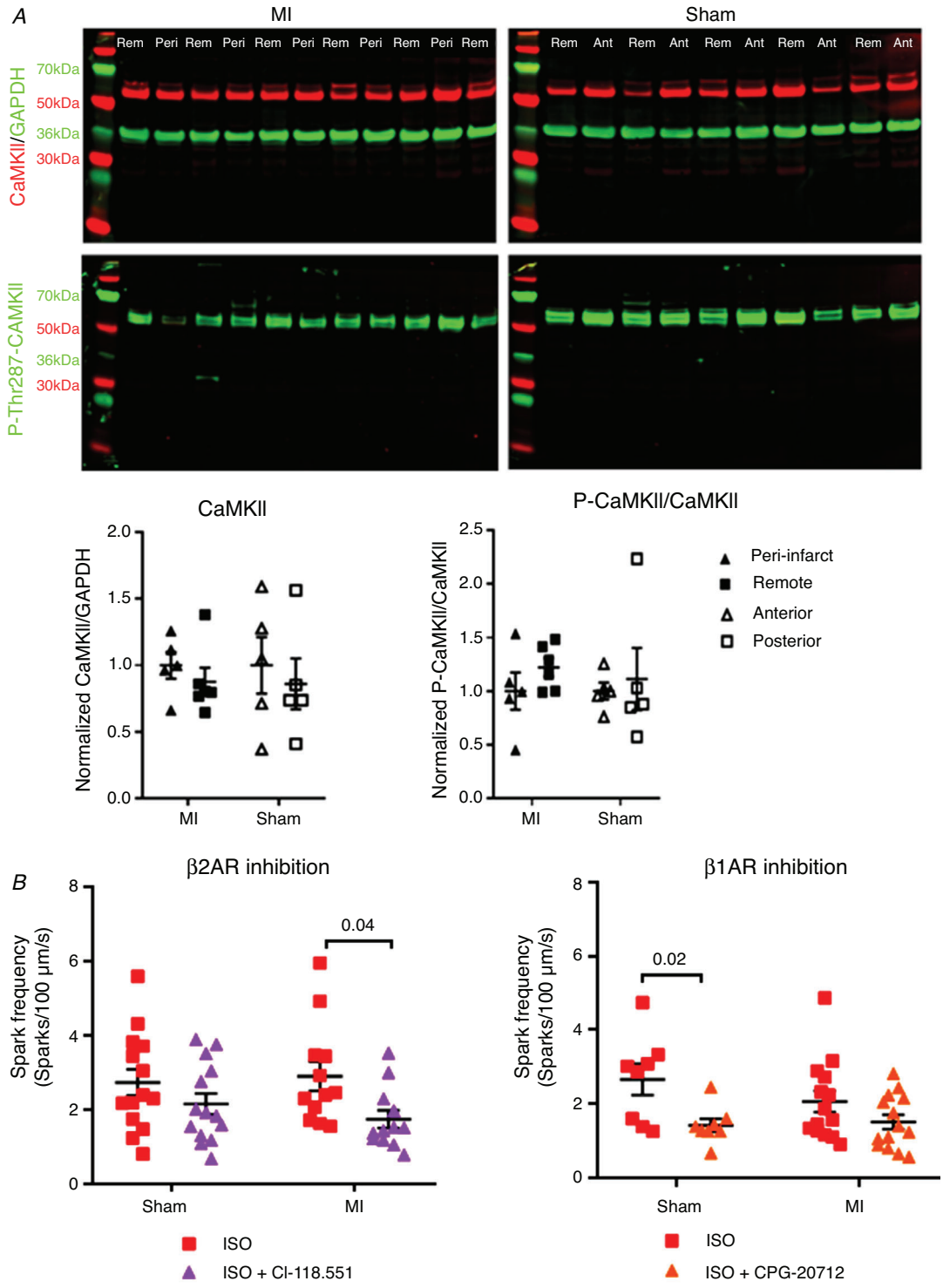

Figure 10. Adrenergic signalling
A, Western blot for CaMKII (55 kDa) and GAPDH (37 kDa) expression and phosphorylated CaMKII (top); total CaMKII was normalized to GAPDH and the level of phosphorylation determined by the ratio of phosphorylated and total CaMKII, with level in remote/posterior normalized to peri-infarct/anterior (bottom), in MI ($N_{pigs} = 6$) and Sham ($N_{pigs} = 5$). Unpaired Student's *t* test between regions. *B*, reduced spark frequency in response to β_1 block (CPG-20712 dihydrochloride, 100 nM) *vs.* β_2 block (ICI-118.551 hydrochloride, 50 nM), in the presence of 10 nM ISO with preconditioning at 0.5 Hz. MI peri-infarct ($n_{cells} = 12–14$; $N_{pigs} = 4–5$) and matched Sham ($n_{cells} = 8–14$; $N_{pigs} = 4–5$) myocytes. Each data point represents one cell; repeated measures two-way ANOVA with Bonferroni *post hoc* testing.

our model at 6 weeks post-MI. These authors studied an end-stage heart failure model (6 months post-MI), where potentially more extensive remodelling will shape regional differences.

In vivo repolarization instability can provide a functional re-entry substrate that adds to the well-known MI structural substrate (De Bakker *et al.* 1993; Ashikaga *et al.* 2007; Ciaccio *et al.* 2015). Computational studies consider generalized myocyte remodelling with AP prolongation and repolarization instability but do not include a region-specific myocyte profile (Pashakhanloo *et al.* 2018).

Here, using MAP recordings we find evidence that post-MI adrenergic stimulation *in vivo* enhances repolarization instability and facilitates arrhythmias specifically in the peri-infarct region. These *in vivo* findings correlate to increased BVR in isolated myocytes from the peri-infarct region, only observed during adrenergic stimulation. The co-incidence of both afterdepolarizations and BVR allows for dual mechanisms of triggered activity, focal as well as micro-reentry, as also proposed for torsade de pointes (Dunnink *et al.* 2017) and suggested by modelling studies (Liu *et al.* 2015).

Cellular mechanisms of repolarization instability and afterdepolarizations

The vulnerability of the peri-infarct zone superimposes on general myocyte remodelling. Hypertrophy and loss of T-tubules are present throughout the surviving LV. These findings are in line with the specific peri-infarct changes in fibrosis, superimposed on general fibroblast activation (Nagaraju *et al.* 2017) and consistent with the recent study in the post-MI mouse heart, identifying specific peri-infarct signalling (van Duijvenboden *et al.* 2019). Reduced Ca^{2+} transient amplitude and rise time at baseline are seen in all regions, and could be due to the loss of T-tubules as well as changes in protein expression and regulation. The gene expression of the hypertrophy marker NPPA was nevertheless higher in the peri-infarct region, suggesting there may a different gene expression programme.

The present study did not compile a functional catalogue of individual currents in the myocytes but agrees with Hegyi *et al.* (2018) that multiple currents are likely to be involved in facilitating re-entry as well as triggered activity, e.g. the reduction in *KCNJ2* will affect repolarization as well as facilitate delayed afterdepolarizations. The data further suggest interaction between spontaneous release events, repolarization and BVR, as previously proposed (Johnson *et al.* 2013). Firstly, we noted a high correlation between cellular DAD incidence and increased BVR. Secondly, after a spontaneous Ca^{2+} release and DAD, the subsequent global Ca^{2+} transient was reduced, often accompanied by APD prolongation. These findings are in line with Ca^{2+}-dependent modulation of the L-type Ca^{2+} current as a factor driving adrenergic-stimulated BVR (Johnson *et al.* 2013; Antoons *et al.* 2015). Reduced inactivation of the L-type Ca^{2+} current would in turn contribute to cellular Ca^{2+} load. Whilst requiring further corroboration, such a mechanism supports the notion that impaired Ca^{2+} handling during adrenergic signalling acts as a central event contributing to both the trigger and the functional substrate for arrhythmias after MI.

Convergence of trigger and substrate in the peri-infarct region through altered adrenergic response

Our data indicate that an altered adrenergic response is likely to define the pro-arrhythmic nature of the peri-infarct myocytes, with a convergence of triggered activity and facilitation of re-entry. We used a low dose of ISO to detect subtle differences in response that could relate to changes in the signalling pathways. At the molecular level, differences in the adrenergic signalling cascade and/or structure could explain the unique vulnerability of the peri-infarct myocytes. Data on their expression at mRNA level suggest a local shift in β_1-AR: β_2-AR stoichiometry and signalling. The different response to β_1-AR block compared to β_2AR is consistent with this notion. Reduced expression of β_1-AR and preserved β_2-AR expression has been observed in heart failure (DeSantiago *et al.* 2008; Lang *et al.* 2015). This altered expression results in different sensitivity and signalling, where β_2-AR signalling becomes dominant in heart failure (Pogwizd *et al.* 2001) and leads to arrhythmias mediated by spontaneous Ca^{2+} release (DeSantiago *et al.* 2008). Recent studies indicate a significant crosstalk between β-AR signalling and CaMKII activation (Curran *et al.* 2007; Dries *et al.* 2016; Shugg *et al.* 2018), presenting CaMKII as a possible downstream mediator of detrimental β-AR signalling after MI. In support of this, CaMKII inhibition reduced DAD incidence and amplitude in peri-infarct myocytes.

Differences in cellular β-AR signalling could also be the result of local re-organization of receptors at the surface and T-tubular membranes (Nikolaev *et al.* 2010). The changes in adrenergic signalling and responses can themselves be consequent on the altered regional innervation and its trophic influence on the myocytes (Habecker *et al.* 2016; Pianca *et al.* 2019).

In vivo, differential nerve sprouting post MI contributes to the arrhythmogenic nature of the border zone (Gardner *et al.* 2015). Neuromodulation and reduction of sympathetic inputs suppress arrhythmias after MI in the pig model (Chui *et al.* 2017) and patients with intractable VT can benefit from bilateral stellectomy (Vaseghi *et al.* 2017). Ischaemia, evoked by adrenergic stimulation,

may superimpose on the vulnerable peri-infarct myocytes and enhance arrhythmic potential. The interactions of the local heterogeneous peri-infarct innervation with varying amounts of circulating catecholamines and other hormones may contribute to additional regional heterogeneity and should be the subject of further investigation.

Implications for arrhythmogenesis and therapy

The findings of the present study underscore the potential benefit for targeting neuro-hormonal, and in particular adrenergic, signalling to prevent arrhythmia and sudden cardiac death after MI, as included in current guidelines (Al-Khatib *et al.* 2018). Our findings additionally support the caution against drugs that challenge an already limited repolarization reserve. Given the residual high risk for arrhythmia post MI, within the time window studied here, novel pharmacological approaches are needed. Our study identifies altered Ca^{2+} handling that can be prevented by CaMKII inhibition, which has also been shown to be beneficial in human cellular and tissue studies (Sossalla *et al.* 2010; Dries *et al.* 2018), and advocates for its potential in post-MI therapy.

Ablative strategies targeting the peri-infarct substrate are effective at treating post-MI arrhythmia but also have limitations (Baldinger *et al.* 2016). Our study highlights the role of myocyte remodelling for both the triggers and functional substrate of the arrhythmia. Therefore, targeting the myocytes through local approaches such as targeted gene therapy (Sasano *et al.* 2006) and exosome targeting (Antes *et al.* 2018) may offer alternative, non-destructive strategies to treat post-MI arrhythmia.

Limitations

The neurotransmitter of adrenergic activation *in vivo* is noradrenaline, activating both α- and β-receptors in heart and vasculature, with a contribution of circulating adrenaline. Here we chose to use isoproterenol to focus on the myocyte responses and to be able to use a similar agent *in vivo* and *in vitro*. Although we could use noradrenaline in isolated myocytes, when applied *in vivo*, peripheral vascular effects and secondary adaptations would confound the cardiac response to noradrenaline. In myocytes, the β-receptor-mediated response has a major role in the calcium changes, hence the choice for ISO as a single agent *in vivo* and *in vitro*.

The current study aimed to record DADs using MAP catheters and this approach did not allow us to definitively correlate the ECG recorded PVC with its site of origin. More comprehensive mapping needs to be included in future studies.

Post-MI remodelling may affect transmural regions differentially and was not investigated in the present study. Cellular studies used the mid-myocardial layers, which constitutes the bulk of the cardiac mass but we did not examine the transmural spectrum.

In the translation of single cell observations to whole heart arrhythmias, factors such as cell coupling and the source-sink mismatch play an important role and could not be resolved in the present study. Additionally, we did not address how multiple cell types contribute to the electrophysiological phenotype, nor individual ionic current remodelling; this needs to be explored in future studies.

Conclusions

Altered myocyte adrenergic responses define the peri-infarct zone as a prominent source of triggered activity and of concomitant repolarization instability, amplifying the potential for re-entry and contributing to the substrate for arrhythmia. This is the result of the unique properties of the peri-infarct myocytes. These findings stimulate further exploration of local therapies targeting myocytes and autonomic modulation.

References

Aimond F, Alvarez JL, Rauzier JM, Lorente P & Vassort G (1999). Ionic basis of ventricular arrhythmias in remodelled rat heart during long-term myocardial infarction. *Cardiovasc Res* **42**, 402–415.

Ajijola OA, Lux RL, Khahera A, Kwon O, Aliotta E, Ennis DB, Fishbein MC, Ardell JL & Shivkumar K (2017). Sympathetic modulation of electrical activation in normal and infarcted myocardium: implications for arrhythmogenesis. *Am J Physiol Heart Circ Physiol* **312**, H608–H621.

Al-Khatib SM, Stevenson WG, Ackerman MJ, Bryant WJ, Callans DJ, Curtis AB, Deal BJ, Dickfeld T, Field ME, Fonarow GC, Gillis AM, Granger CB, Hammill SC, Hlatky MA, Joglar JA, Kay GN, Matlock DD, Myerburg RJ & Page RL (2018). 2017 AHA/ACC/HRS guideline for management of patients with ventricular arrhythmias and the prevention of sudden cardiac death: Executive summary: A Report of the American College of Cardiology/American Heart Association Task Force on Clinical Practice Gui. *Heart Rhythm* **15**, e190–e252.

Antes TJ, Middleton RC, Luther KM, Ijichi T, Peck KA, Liu WJ, Valle J, Echavez AK & Marbán E (2018). Targeting extracellular vesicles to injured tissue using membrane cloaking and surface display. *J Nanobiotechnol* **16**, 1–15.

Antoons G, Johnson DM, Dries E, Santiago DJ, Ozdemir S, Lenaerts I, Beekman JDM, Houtman MJC, Sipido KR & Vos MA (2015). Calcium release near L-type calcium channels promotes beat-to-beat variability in ventricular myocytes from the chronic AV block dog. *J Mol Cell Cardiol* **89**, 326–334.

Ashikaga H, Sasano T, Dong J, Zviman MM, Evers R, Hopenfeld B, Castro V, Helm RH, Dickfeld T, Nazarian S, Donahue JK, Berger RD, Calkins H, Abraham MR, Marbán E, Lardo AC, McVeigh ER & Halperin HR (2007). Magnetic resonance-based anatomical analysis of scar-related ventricular tachycardia: Implications for catheter ablation. *Circ Res* **101**, 939–947.

Baba S, Dun W, Cabo C & Boyden PA (2005). Remodelling in cells from different regions of the reentrant circuit during ventricular tachycardia. *Circulation* **112**, 2386–2396.

Baldinger SH, Stevenson WG & John RM (2016). Ablation of ischemic ventricular tachycardia: Evidence, techniques, results, and future directions. *Curr Opin Cardiol* **31**, 29–36.

Belevych AE, Terentyev D, Terentyeva R, Ho HT, Gyorke I, Bonilla IM, Carnes CA, Billman GE & Györke S (2012). Shortened Ca^{2+} signaling refractoriness underlies cellular arrhythmogenesis in a postinfarction model of sudden cardiac death. *Circ Res* **110**, 569–577.

Bogun F, Crawford T, Chalfoun N, Kuhne M, Sarrazin JF, Wells D, Good E, Jongnarangsin K, Oral H, Chugh A, Pelosi F & Morady F (2008). Relationship of frequent postinfarction premature ventricular complexes to the reentry circuit of scar-related ventricular tachycardia. *Heart Rhythm* **5**, 367–574.

Bogun F, Good E, Reich S, Elmouchi D, Igic P, Tschopp D, Dey S, Wimmer A, Jongnarangsin K, Oral H, Chugh A, Pelosi F & Morady F (2006). Role of Purkinje fibers in post-infarction ventricular tachycardia. *J Am Coll Cardiol* **48**, 2500–2507.

Cao JM, Chen LS, KenKnight BH, Ohara T, Lee MH, Tsai J, Lai WW, Karagueuzian HS, Wolf PL, Fishbein MC & Chen PS (2000). Nerve sprouting and sudden cardiac death. *Circ Res* **86**, 816–821.

Christensen MD, Dun W, Boyden PA, Anderson ME, Mohler PJ & Hund TJ (2009). Oxidized calmodulin kinase II regulates conduction following myocardial infarction: A computational analysis. *PLoS Comput Biol* **5**, e1000583.

Chui RW, Buckley U, Rajendran PS, Vrabec T, Shivkumar K & Ardell JL (2017). Bioelectronic block of paravertebral sympathetic nerves mitigates post-myocardial infarction ventricular arrhythmias. *Heart Rhythm* **14**, 1665–1672.

Ciaccio EJ, Coromilas J, Ashikaga H, Cervantes DO, Wit AL, Peters NS, McVeigh ER & Garan H (2015). Model of unidirectional block formation leading to reentrant ventricular tachycardia in the infarct border zone of postinfarction canine hearts. *Comput Biol Med* **62**, 254–263.

Ciaccio EJ, Coromilas J, Wit AL, Peters NS & Garan H (2018). Source-sink mismatch causing functional conduction block in re-entrant ventricular tachycardia. *JACC Clin Electrophysiol* **4**, 1–16.

Cronin EM, Bogun FM, Maury P, Peichl P, Chen M, Namboodiri N, Aguinaga L, Leite LR, Al-Khatib SM, Anter E, Berruezo A, Callans DJ, Chung MK, Cuculich P, d'Avila A, Deal BJ, Della Bella P, Deneke T, Dickfeld TM, Hadid C, Haqqani HM, Kay GN, Latchamsetty R, Marchlinski F, Miller JM, Nogami A, Patel AR, Pathak RK, Sáenz Morales LC, Santangeli P, Sapp JL, Sarkozy A, Soejima K, Stevenson WG, Tedrow UB, Tzou WS, Varma N & Zeppenfeld K (2019). 2019 HRS/EHRA/APHRS/LAHRS expert consensus statement on catheter ablation of ventricular arrhythmias. *Europace* **21**, 1143–1144.

Curran J, Hinton MJ, Ríos E, Bers DM & Shannon TR (2007). B-adrenergic enhancement of sarcoplasmic reticulum calcium leak in cardiac myocytes is mediated by calcium/calmodulin-dependent protein kinase. *Circ Res* **100**, 391–398.

De Bakker JMT, Van Capelle FJL, Janse MJ, Tasseron S, Vermeulen JT, De Jonge N & Lahpor JR (1993). Slow conduction in the infarcted human heart: "Zigzag" course of activation. *Circulation* **88**, 915–926.

De Groot SHM, Vos MA, Gorgels APM, Leunissen JDM, Van Der Steld BJ & Wellens HJJ (1995). Combining monophasic action potential recordings with pacing to demonstrate delayed afterdepolarizations and triggered arrhythmias in the intact heart: Value of diastolic slope. *Circulation* **92**, 2697–2704.

DeSantiago J, Ai X, Islam M, Acuna G, Ziolo MT, Donald M & Pogwizd SM (2008). Arrhythmogenic effects of β_2-adrenergic stimulation in the failing heart are due to enhanced SR Ca load. *Circ Res* **102**, 1389–1397.

Dries E, Santiago DJ, Gilbert G, Lenaerts I, Vandenberk B, Nagaraju CK, Johnson DM, Holemans P, Roderick HL, Macquaide N, Claus P & Sipido KR (2018). Hyperactive ryanodine receptors in human heart failure and ischemic cardiomyopathy reside outside of couplons. *Cardiovasc Res* **114**, 1512–1524.

Dries E, Santiago DJ, Johnson DM, Gilbert G, Holemans P, Korte SM, Roderick Hl & Sipido KR (2016). Calcium/calmodulin-dependent kinase II and nitric oxide synthase 1-dependent modulation of ryanodine receptors during β-adrenergic stimulation is restricted to the dyadic cleft. *J Physiol* **65**, 461–468.

Dun W, Danilo P, Mohler PJ & Boyden PA (2018). Microtubular remodelling and decreased expression of Nav1.5 with enhanced EHD4 in cells from the infarcted heart. *Life Sci* **201**, 72–80.

Dun W, Lowe JS, Wright P, Hund TJ, Mohler PJ & Boyden PA (2013). Ankyrin-G participates in INa remodelling in myocytes from the border zones of infarcted canine heart. *PLoS One* **8**, 1–13.

Dunnink A, Stams TRG, Bossu A, Meijborg VMF, Beekman JDM, Wijers SC, De Bakker JMT & Vos MA (2017). Torsade de pointes arrhythmias arise at the site of maximal heterogeneity of repolarization in the chronic complete atrioventricular block dog. *Europace* **19**, 858–865.

Franz MR (1999). Current status of monophasic action potential recording: Theories, measurements and interpretations. *Cardiovasc Res* **41**, 25–40.

Galan DT, Bito V, Claus P, Holemans P, Abi-Char J, Nagaraju CK, Dries E, Vermeulen K, Ventura-Clapier R, Sipido KR & Driesen RB (2016). Reduced mitochondrial respiration in the ischemic as well as in the remote nonischemic region in postmyocardial infarction remodelling. *Am J Physiol Heart Circ Physiol* **311**, H1075–H1090.

Gardner R, Wang L, Lang B, Cregg J, Dunbar C, Woodward W, Silver J, Ripplinger C & Habecker B (2015). Targeting protein tyrosine phosphatase σ after myocardial infarction restores cardiac sympathetic innervation and prevents arrhythmias. *Nat Commun* **6**, 1–9.

Gonca E (2015). Comparison of thiopental and ketamine+xylazine anaesthesia in ischemia/reperfusion-induced arrhythmias in rats. *Turkish J Med Sci* **45**, 1413–1420.

Grundy D (2015). Principles and standards for reporting animal experiments in *The Journal of Physiology* and *Experimental Physiology*. *J Physiol* **593**, 2547–2549.

Habecker BA, Anderson ME, Birren SJ, Fukuda K, Herring N, Hoover DB, Kanazawa H, Paterson DJ & Ripplinger CM (2016). Molecular and cellular neurocardiology: development, and cellular and molecular adaptations to heart disease. *J Physiol* **594**, 3853–3875.

Hayashi M, Shimizu W & Albert CM (2015). The spectrum of epidemiology underlying sudden cardiac death. *Circulation* **116**, 1887–1906.

Hegyi B, Bossuyt J, Griffiths LG, Shimkunas R, Coulibaly Z, Jian Z, Grimsrud KN, Sondergaard CS, Ginsburg KS, Chiamvimonvat N, Belardinelli L, Varró A, Papp JG, Pollesello P, Levijoki J, Izu LT, Boyd WD, Bányász T, Bers DM & Chen-Izu Y (2018). Complex electrophysiological remodelling in postinfarction ischemic heart failure. *Proc Natl Acad Sci U S A* **115**, E3036–E3044.

Heidbüchel H, Hoogsteen J, Fagard R, Vanhees L, Ector H, Willems R & Van Lierde J (2003). High prevalence of right ventricular involvement in endurance athletes with ventricular arrhythmias: Role of an electrophysiologic study in risk stratification. *Eur Heart J* **24**, 1473–1480.

Hirose M, Stuyvers BD, Dun W, ter Keurs HEDJ & Boyden PA (2008). Function of Ca^{2+} release channels in Purkinje cells that survive in the infarcted canine heart: a mechanism for triggered Purkinje ectopy. *Circ Arrhythm Electrophysiol* **1**, 387–395.

Johnson DM, Heijman J, Bode EF, Greensmith DJ, Van Der Linde H, Abi-Gerges N, Eisner DA, Trafford AW & Volders PGA (2013). Diastolic spontaneous calcium release from the sarcoplasmic reticulum increases beat-to-beat variability of repolarization in canine ventricular myocytes after β-adrenergic stimulation. *Circ Res* **112**, 246–256.

Lang D, Holzem K, Kang C, Xiao M, Hwang HJ, Ewald GA, Yamada KA & Efimov IR (2015). Arrhythmogenic remodelling of β_2 versus β_1 adrenergic signaling in the human failing heart. *Circ Arrhythm Electrophysiol* **8**, 409–419.

Lerma C, Gorelick A, Ghanem RN, Glass L & Huikuri HV (2013). Patterns of ectopy leading to increased risk of fatal or near-fatal cardiac arrhythmia in patients with depressed left ventricular function after an acute myocardial infarction. *Europace* **15**, 1304–1312.

Liu MB, De Lange E, Garfinkel A, Weiss JN & Qu Z (2015). Delayed afterdepolarizations generate both triggers and a vulnerable substrate promoting reentry in cardiac tissue. *Heart Rhythm* **12**, 2115–2124.

Lue W & Boyden P (1992). Abnormal electrical properties of myocytes from chronically infarted canine heart. *Circulation* **85**, 1175–1188.

Marrouche NF, Verma A, Wazni O, Schweikert R, Martin DO, Saliba W, Kilicaslan F, Cummings J, Burkhardt JD, Bhargava M, Bash D, Brachmann J, Guenther J, Hao S, Beheiry S, Rossillo A, Raviele A, Themistoclakis S & Natale A (2004). Mode of initiation and ablation of ventricular fibrillation storms in patients with ischemic cardiomyopathy. *J Am Coll Cardiol* **43**, 1715–1720.

Moore HJ & Franz MR (2007). Monophasic action potential recordings in humans. *J Cardiovasc Electrophysiol* **18**, 787–790.

Nagaraju CK, Dries E, Popovic N, Singh AA, Haemers P, Roderick HL, Claus P, Sipido KR & Driesen RB (2017). Global fibroblast activation throughout the left ventricle but localized fibrosis after myocardial infarction. *Sci Rep* **7**, 1–14.

Nikolaev VO, Moshkov A, Lyon AR, Miragoli M, Novak P, Paur H, Lohse MJ, Korchev YE, Harding SE & Gorelik J (2010). β_2-Adrenergic receptor redistribution in heart failure changes cAMP compartmentation. *Science* **327**, 1653–1658.

Pashakhanloo F, Herzka DA, Halperin H, McVeigh ER & Trayanova NA (2018). Role of 3-dimensional architecture of scar and surviving tissue in ventricular tachycardia: insights from high-resolution ex vivo porcine models. *Circ Arrhythmia Electrophysiol* **11**, 1–12.

Pianca N, Di Bona A, Lazzeri E, Costantini I, Franzoso M, Prando V, Armani A, Rizzo S, Fedrigo M, Angelini A, Basso C, Pavone FS, Rubart M, Sacconi L, Zaglia T & Mongillo M (2019). Cardiac sympathetic innervation network shapes the myocardium by locally controlling cardiomyocyte size through the cellular proteolytic machinery. *J Physiol* **597**, 3639–3656.

Pogwizd SM, Schlotthauer K, Li L, Yuan W & Bers DM (2001). Arrhythmogenesis and contractile dysfunction in heart failure: roles of sodium-calcium exchange, inward rectifier potassium current, and residual beta-adrenergic responsiveness. *Circ Res* **88**, 1159–1167.

Prakosa A, Arevalo HJ, Deng D, Boyle PM, Nikolov PP, Ashikaga H, Blauer JJE, Ghafoori E, Park CJ, Blake RC, Han FT, MacLeod RS, Halperin HR, Callans DJ, Ranjan R, Chrispin J, Nazarian S & Trayanova NA (2018). Personalized virtual-heart technology for guiding the ablation of infarct-related ventricular tachycardia. *Nat Biomed Eng* **2**, 732–740.

Priori SG, Mantica M & Schwartz PJ (1988). Delayed afterdepolarizations elicited *in vivo* by left stellate ganglion stimulation. *Circulation* **78**, 178–185.

Rajendran PS, Nakamura K, Ajijola OA, Vaseghi M, Armour JA, Ardell JL & Shivkumar K (2016). Myocardial infarction induces structural and functional remodelling of the intrinsic cardiac nervous system. *J Physiol* **594**, 321–341.

Rivas N, Dhruvakumar S, Mainigi SK, Smith T, Gerstenfeld EP & Marchlinski FE (2009). Ventricular premature depolarizations triggered by incremental dose isoproterenol infusion: common electrocardiographic features. *J Interv Card Electrophysiol* **25**, 43–51.

Saeed M, Link MS, Mahapatra S, Mouded M, Tzeng D, Jung V, Contreras R, Swygman C, Homoud M, Mark Estes NA & Wang PJ (2000). Analysis of intracardiac electrograms showing monomorphic ventricular tachycardia in patients with implantable cardioverter-defibrillators. *Am J Cardiol* **85**, 580–587.

Sasano T, McDonald AD, Kikuchi K & Donahue JK (2006). Molecular ablation of ventricular tachycardia after myocardial infarction. *Nat Med* **12**, 1256–1258.

Shimizu W, Ohe T, Kurita T, Takaki H, Aihara N, Kamakura S, Matsuhisa M & Shimomura K (1991). Early afterdepolarizations induced by isoproterenol in patients with congenital long QT syndrome. *Circulation* **84**, 1915–1923.

Shugg T, Johnson DE, Shao M, Lai X, Witzmann F, Cummins TR, Rubart-Von-der Lohe M, Hudmon A & Overholser BR (2018). Calcium/calmodulin-dependent protein kinase II regulation of IKs during sustained β-adrenergic receptor stimulation. *Heart Rhythm* **15**, 895–904.

Sossalla S, Fluschnik N, Schotola H, Ort KR, Neef S, Schulte T, Wittköpper K, Renner A, Schmitto JD, Gummert J, El-Armouche A, Hasenfuss G & Maier LS (2010). Inhibition of elevated Ca^{2+}/calmodulin-dependent protein kinase II improves contractility in human failing myocardium. *Circ Res* **107**, 1150–1161.

Thomsen MB, Verduyn SC, Stengl M, Beekman JDM, de Pater G, van Opstal J, Volders PGA & Vos MA (2004). Increased short-term variability of repolarization predicts *d*-sotalol-induced torsades de pointes in dogs. *Circulation* **110**, 2453–2459.

Vandesompele J, De Preter K, Pattyn F, Poppe B, Van Roy N & De Paepe A (2002). Accurate normalization of real-time quantitative RT-PCR data by geometric averaging of multiple internal control genes. *Genome Biol* **3**, research0034.1.

van Duijvenboden K, de Bakker DEM, Man JCK, Janssen R, Günthel M, Hill MC, Hooijkaas IB, van der Made I, van der Kraak PH, Vink A, Creemers EE, Martin JF, Barnett P, Bakkers J & Christoffels VM (2019). Conserved NPPB+ border zone switches from MEF2 to AP-1 driven gene program. *Circulation* **140**, 864–879.

Vaseghi M, Barwad P, Malavassi Corrales FJ, Tandri H, Mathuria N, Shah R, Sorg JM, Gima J, Mandal K, Sàenz Morales LC, Lokhandwala Y & Shivkumar K (2017). Cardiac sympathetic denervation for refractory ventricular arrhythmias. *J Am Coll Cardiol* **69**, 3070–3080.

Verma A, Marrouche NF, Schweikert RA, Saliba W, Wazni O, Cummings J, Abdul-Karim A, Bhargava M, Burkhardt JD, Kilicaslan F, Martin DO & Natale A (2005). Relationship between successful ablation sites and the scar border zone defined by substrate mapping for ventricular tachycardia post-myocardial infarction. *J Cardiovasc Electrophysiol* **16**, 465–471.

Wong SS, Bassett AL, Cameron JS, Epstein K, Kozlovskis P & Myerburg RJ (1982). Dissimilarities in the electrophysiological abnormalities of lateral border and central infarct zone cells after healing of myocardial infarction in cats. *Circ Res* **51**, 486–493.

Xing D & Martins JB (2004). Triggered activity due to delayed afterdepolarizations in sites of focal origin of ischemic ventricular tachycardia. *Am J Physiol Heart Circ Physiol* **287**, H2078–H2084.

Additional information

Competing interests

R.W. has received research funding from Biotronik, Boston Scientific and Medtronic and speakers and consultancy fees from Biotronik, Boston Scientific, Medtronic, St Jude Medical and Sorin. This has no influence on the exploratory study reported here and is therefore not a competing interest.

Author contributions

K.R.S., R.W., P.C., H.L.R., E.D., M.A. contributed to conception and design of the work; K.R.S., R.W., P.C., H.L.R., E.D., M.A., B.V., D.M.J., G.G., C.K.N., R.D.P., M.Ab., D.J.S. were involved in acquiring, analysing or interpreting the data of this work; K.R.S., R.W., P.C., H.L.R., E.D., M.A., B.V., D.M.J., G.G., C.K.N., R.D.P., M.Ab., D.J.S. were involved in drafting the work or revising it. All authors revised and approved the final version of the manuscript. All persons designated as author, qualify for authorship and are listed.

Funding

This work was supported by the Fund for Scientific Research-Flanders (FWO projects G.0617.09 and G.0918.15 to K.R.S., FWO Project grant G08861N and FWO Odysseus Project 90 663 to H.L.R.; FWO Senior Clinical Investigator to R.W.; FWO postdoctoral fellowships to E.D., D.M.J. and G.G.; FWO PhD fellowship to M.A.), and by Horizon 2020 MSCA-IF-2016-752824 to M.Ab.

Acknowledgements

We thank Patricia Holemans, Roxane Menten and Sofie van Soest for technical assistance.

Keywords

animal models of human disease, arrhythmias, autonomic nervous system, calcium cycling

Supporting information

Additional supporting information may be found online in the Supporting Information section at the end of the article.

Statistical Summary Document